Bifurcations of hidden orbits in discontinuous maps

Viktor Avrutin[1] **and Mike R. Jeffrey**[2]

[1] Institute for Systems Theory and Automatic Control, University of Stuttgart, Pfaffenwaldring 9, 70550 Stuttgart, Germany

E-mail: `Avrutin@ist.uni-stuttgart.de`

[2] Department of Engineering Mathematics, University of Bristol, Ada Lovelace Building, Bristol BS8 1TW, UK

E-mail: `Mike.Jeffrey@bristol.ac.uk`

Abstract. One-dimensional maps with discontinuities are known to exhibit bifurcations somewhat different to those of continuous maps. Freed from the constraints of continuity, and hence from the balance of stability that is maintained through fold, flip, and other standard bifurcations, the attractors of discontinuous maps can appear as if from nowhere, and change period or stability almost arbitrarily. But in fact this is misleading, and if one includes states inside the discontinuity in the map, highly unstable "hidden orbits" are created that have iterates on the discontinuity. These populate the bifurcation diagrams of discontinuous maps with just the necessary unstable branches to make them resemble those of continuous maps, namely fold, flip, and other familiar bifurcations. Here we analyse such bifurcations in detail, focussing first on folds and flips, then on bifurcations characterized by creating infinities of orbits, chaotic repellers, and infinite accumulations of sub-bifurcations. We show the role that hidden orbits play, and how they capture the topological structures of continuous maps with steep branches. This suggests both that a more universal dynamical systems theory marrying continuous and discontinuous systems is possible, and shows how discontinuities can be used to approximate steep jumps in continuous systems without losing any of their topological structure.

Keywords: discontinuous maps, steep maps, stiff maps, border collision bifurcations, hidden orbits, unstable orbits

Submitted to: *Nonlinearity*

1. Motivation

Discontinuous maps play a widespread and important role in dynamical systems. If two states of a system are able to lie arbitrary close, but subsequently evolve along significantly different

trajectories, then a map that integrates along those trajectories is necessarily discontinuous. The source of such divergence is typically the straddling of some separatrix. One example is a stable manifold that determines whether trajectories pass to one side or another of a saddle equilibrium, in a differentiable system such as the Lorenz or Cherry flows [1, 2, 3, 4]. Another key example is a grazing orbit that determines whether trajectories hit or miss a control surface at which a discontinuous action is triggered, commonly found in electronic control relays triggered by a reference signal [5, 6, 7], homeostatic models where sleeping or waking are triggered at distinct hormone thresholds [30], and other switching processes that occur on a faster time scale than the system they affect, such as cell mitosis [9].

Although derivable from continuous systems, the dynamics of discontinuous maps differ fundamentally from those of continuous maps. Freed from the constraints of continuity, they are seemingly able to exhibit counterintuitive behaviours. Attractors can appear or disappear, and change stability or periodicity, in almost arbitrary ways that are not possible in continuous maps; see e.g. [10, 11, 12]. A fixed point or periodic orbit coming into contact with a discontinuity can create global bifurcations, involving orbital structures reaching far from the site of the bifurcation, such as broad band chaotic attractors [15].

In [16], however, it was suggested that one could sensibly define trajectories that posses one or more iterates inside the discontinuity — dubbed *hidden orbits* — whose existence would render the behaviours of discontinuous maps commensurate with their continuous cousins. The purpose of [16] was merely to show the existence of hidden orbits and their significance in a typical discontinuity-induced bifurcation sequence. In the present paper, we begin the systematic study of bifurcations that involve hidden orbits. By doing so, we begin to understand the connection between the behaviours of discontinuous and continuous maps, and see that a unified theory of their bifurcations may in fact be possible. This shows moreover that nonlinear systems can be approximated by discontinuous maps without changing the topology of the bifurcations they exhibit, something that is not possible without hidden orbits, as we shall see.

When dealing with discontinuous maps, the question arises as to how the map is to be defined at the point of discontinuity. Historically this question has not been considered deeply, mostly because this definition does not affect the location of bifurcations in the map or the structures of orbits that surround the discontinuity. It has therefore been common to assign a specific value to the function at the point of discontinuity, motivated by convenience or modeling application, and specific to the system under consideration. For example, in maps derived from homoclinic connections in flows, it is natural to define the map as having a unique unstable fixed point at the discontinuity. In a system with a relay control, it is reasonable to define the map at the discontinuity by the limiting value of the function corresponding to the switching. In classification studies, it has been common to choose either the limiting value from one side of the discontinuity, or the mid-value (the half-sum of the limiting values), or else to omit the discontinuity altogether and leave the map undefined

there.

In [17], for example, particular values of the map are permitted (namely $f_{\mathcal{L}}(0)$, $f_{\mathcal{R}}(0)$, and their midpoint), that yield unstable orbits with points on the discontinuity, contributing to a 'period doubling without flip' bifurcation. In [18], so-called 'discontinuous crossings' are identified in an impact system, and it is noted that these are "not periodic solutions or equilibria" of the system of interest. All such solutions are precisely what we elevate and generalize here to precisely the status of periodic solutions or equilibria, albeit highly unstable, but nonetheless important to a dynamical understanding of the system.

All of these different ways of defining a map at a discontinuity are valid to address specific problems, but none of them is general or definitive. In fact none of these approaches is satisfactory in the sense that they neglect the highly unstable influence of having a steep — indeed vertical — branch in the map. Particularly in applications where the discontinuous map is meant to approximate a continuous system, neglecting the discontinuity changes the topology of the state space by removing an entire set of states that generates unstable cycles.

In [16] it was suggested that much would be gained by defining the map at the discontinuity to be set-valued. In this way, the function remains discontinuous, but becomes *connected* in the sense that there exist a continuum of states connecting the branches of the map across the discontinuity. Although the map is then multi-valued at the discontinuity, by treating iterates of the map that lie on this set naively like any other, one obtains *hidden* orbits that have iterates inside the discontinuity. It was suggested in [16] that these hidden orbits were precisely the unstable orbits needed to restore the bifurcation structures that would be observed in an approximating continuous map. A specific example was given showing how a previously familiar period incrementing sequence becomes populated by unstable hidden cycles, and these reveal the border collision bifurcations — in which branches of attractors are born as if from nowhere — to be nothing but standard nonsmooth flip and fold bifurcations.

Rather than consider an extensive list of the many possible bifurcations in discontinuous maps, we distinguish three key 'orders' of bifurcation, namely those that involve only finitely many periodic orbits, those in which infinitely many branches of periodic orbits issue from the bifurcation point, and those in which the primary bifurcation point is just the accumulation point of infinitely many bifurcation sub-sequences. For each of these we show how they are re-interpreted in familiar standard concepts when hidden orbits are taken into account, and thereby show how nonlinear systems can be approximated by discontinuous maps in a more complete way than it is commonly done. These steps also provide the foundations for a more extensive re-consideration of the bifurcations of discontinuous maps in the presence of hidden orbits.

To help interpret hidden orbits and their role in approximating nonlinear maps, we will distinguish four different approximations of the same system: a **discontinuous map** whose graph has a jump between its left and right branches at $x = 0$, a **connected map**

which duplicates the discontinuous map for $x \neq 0$ but connects its two branches with a vertical branch at $x = 0$, a **continuous map** that approximates the vertical branch by a steep but finite gradient, and a **smooth map** that approximates all of these by an infinitely differentiable map.

In summary, for connected maps we show:

(i) in bifurcations that involve finite number of periodic orbits only, hidden orbits provide unstable branches necessary to recognise discontinuity-induced bifurcations as familiar bifurcations such as a flip or fold,

(ii) in bifurcations that involve infinite numbers of periodic orbits, concatenations of hidden orbits provide the wide patterns of repelling periodic and aperiodic orbits to unify them with bifurcations known in continuous maps,

(iii) in bifurcations that occur at accumulation points of infinitely crowded sequences of bifurcations, hidden orbits restore the complete sequences found in period adding sequences in continuous maps, and provide an easy way to calculate their unstable orbits.

We also relate these to the equivalent bifurcations in discontinuous, continuous, and smooth maps, to see the unstable dynamics within them corresponding to hidden orbits.

In section 4, section 5, and section 6, in turn, we will study specific examples of the three bifurcation scenarios (i)-(iii). In this respect, our purpose in this paper is modest, not to construct a general theory of hidden orbits, since the concept was only introduced recently in [16], rather our purpose is to provide prototypes and a basic understanding that can be made more general and rigorous in future work. For this purpose it is useful to base the study around a piecewise linear map, whose orbits can be found explicitly and whose bifurcations have been extensively studied. For the same purpose we focus on bifurcations as a single parameter is varied, in this case the size of the discontinuity, rather than attempt to classify all bifurcations of these maps. While it is tempting to immediately seek more general results, they will necessarily be more abstract and topological in nature, and more complex, as the range of different map classes and types of bifurcation phenomena is far greater in nonsmooth maps than in smooth maps (though our work here suggests that this is a distinction that could be narrowed in the future). continuous maps the bifurcations exhibited bear a complex relationship to map classes defined by their slopes and modality. It is precisely to gain insight despite these complexities, that we focus on the three scenarios (i)-(iii) here.

The remainder of this paper is organized as follows. In section 2, we define four prototypes we will use to study discontinuous maps and related continuous or smooth maps. Hidden orbits, which can be used to study discontinuous maps, are defined in section 3. The main results of the paper follow in sections 4 to 7, setting out the role of hidden orbits in bifurcation scenarios giving examples of types (i)-(iii) above.

In section 4, we look at two successive border collision bifurcations in a monotonic map,

which are revealed to to be just familiar nonsmooth fold and flip bifurcations once hidden orbits are included. In section 5, we look at a bifurcation that produces infinitely many hidden periodic orbits in a unimodal map. In section 6, we show the role played by hidden orbits in a period adding sequence in a bimodal map. We draw together these results in section 7 and discuss their significance for both the study of discontinuous maps, and the approximation of smooth maps with steep transitions, ending with some forward looking remarks in section 8.

2. Definition of the map

In each part of the paper below, we will take a prototype discontinuous map, then consider a connected map, continuous map, and smooth map, derived from it (see Fig. 1). We use these to study the role of hidden orbits (in the connected map) and their unstable counterparts (in the continuous and smooth maps). Let us begin by defining these four map types below.

2.1. The discontinuous map

Consider the one-dimensional map defined by

$$x_{n+1} = f(x_n) = \begin{cases} f_{\mathcal{L}}(x_n) = a_{\mathcal{L}} x_n + \mu_{\mathcal{L}} & \text{if} \quad x_n < 0 \\ f_{\mathcal{R}}(x_n) = a_{\mathcal{R}} x_n + \mu_{\mathcal{R}} & \text{if} \quad x_n > 0 \end{cases} \tag{1}$$

for some parameters $a_{\mathcal{L}}, a_{\mathcal{R}}, \mu_{\mathcal{L}}, \mu_{\mathcal{R}}$, where in general $f_{\mathcal{L}}(0) \neq f_{\mathcal{R}}(0)$, i.e. $\mu_{\mathcal{L}} \neq \mu_{\mathcal{R}}$. An example is given in Fig. 1(a).

We refer to this as the **discontinuous map**, noting that its value is undefined at $x = 0$. Such maps have been extensively investigated in [11, 10, 12]. A unique value may be assigned at $x_n = 0$, for example the right or left limiting values $f(0) = f_{\mathcal{R}}(0)$ or $f(0) = f_{\mathcal{L}}(0)$, or the midpoint $f(0) = [f_{\mathcal{R}}(0) + f_{\mathcal{L}}(0)]/2$, without substantially altering our analysis below.

2.2. The connected map

We define the **connected map** as the augmented version of (1) given by

$$\begin{aligned} x_{n+1} \; &= f(x_n) = \begin{cases} f_{\mathcal{L}}(x_n) \; = a_{\mathcal{L}} x_n + \mu_{\mathcal{L}} & \text{if} \quad x_n < 0 \,, \\ f_{\mathcal{R}}(x_n) \; = a_{\mathcal{R}} x_n + \mu_{\mathcal{R}} & \text{if} \quad x_n > 0 \,, \end{cases} \\ x_{n+1} \; &\in J = [\min\{f_{\mathcal{R}}(0), f_{\mathcal{L}}(0)\}, \max\{f_{\mathcal{R}}(0), f_{\mathcal{L}}(0)\}] \quad \text{if} \quad x_n = 0 \,, \end{aligned} \tag{2}$$

see Fig. 1(b). For convenience the vertical branch of the function f is denoted by $f_{\mathcal{C}}$, taking a range of values $f_{\mathcal{C}}(0) \in J$, where obviously

$$f_{\mathcal{C}}^{-1}(x) = 0 \qquad \forall x \in J.$$

We should emphasize that the map (2) is discontinuous, like the map (1), but now the branches $f_{\mathcal{L}}$ and $f_{\mathcal{R}}$ are connected across the discontinuity via a vertical branch $f_{\mathcal{C}}$..

By definition, the map (2) is set-valued at the discontinuity. Set-valued maps have been studied by many authors, see e.g. [13, 14], but to our knowledge they have never been applied within the scope of bifurcation analysis of discontinuous maps. As we will see, they can successfully be applied for this purpose, as their dynamics is at once richer and yet more standard than that of discontinuous maps similar to map (1).

2.3. The continuous map

We define the **continuous map** by the piecewise linear function

$$x_{n+1} = f(x_n) = \begin{cases} f_{\mathcal{L}}(x) = a_{\mathcal{L}}x + \mu_{\mathcal{L}} & \text{if} \quad x \leqslant d_{\mathcal{L}}, \\ f_{\mathcal{M}}(x) = a_{\mathcal{M}}x + \mu_{\mathcal{M}} & \text{if} \quad d_{\mathcal{L}} \leqslant x \leqslant d_{\mathcal{R}}, \\ f_{\mathcal{R}}(x) = a_{\mathcal{R}}x + \mu_{\mathcal{R}} & \text{if} \quad x \geqslant d_{\mathcal{R}}, \end{cases} \tag{3}$$

as shown in Fig. 1(c), which coincides with (2) everywhere except for a sufficiently small interval $(d_{\mathcal{L}}, d_{\mathcal{R}})$ with $d_{\mathcal{L}} < 0 < d_{\mathcal{R}}$. To ensure the continuity of (3) at the border points $x = d_{\mathcal{L}}, d_{\mathcal{R}}$, we impose the additional condition

$$a_{\mathcal{M}} = \frac{\mu_{\mathcal{R}} - \mu_{\mathcal{L}} + a_{\mathcal{R}}d_{\mathcal{R}} - a_{\mathcal{L}}d_{\mathcal{L}}}{d_{\mathcal{R}} - d_{\mathcal{L}}}, \quad \mu_{\mathcal{M}} = \frac{(a_{\mathcal{L}} - a_{\mathcal{R}})\, d_{\mathcal{L}}d_{\mathcal{R}} + \mu_{\mathcal{L}}d_{\mathcal{R}} - \mu_{\mathcal{R}}d_{\mathcal{L}}}{d_{\mathcal{R}} - d_{\mathcal{L}}}$$

For an overview of the bifurcation structures in map (3) we direct the reader to [19, 20].

2.4. The smooth map

Lastly we consider a map that smoothly transitions between the functions $f_{\mathcal{L}}$ and $f_{\mathcal{R}}$ from (1), in the form

$$x_{n+1} = f_{\mathcal{L}}(x) \cdot (1 - g(x)) + f_{\mathcal{R}}(x) \cdot g(x) \tag{4}$$

which we refer to as the **smooth map**, where the function g is some smooth sigmoid transitioning between $g = 0$ and 1 as x changes sign, which we take as

$$g(x) = \frac{1}{1 + e^{-\frac{x}{\varepsilon^2}}}$$

for small ε (see Fig. 1(d)).

2.5. The different maps compared

The four maps defined above clearly all possess similarities in their dynamics, but it is the subtle differences associated with their differing continuity or differentiability that interests us. By construction, any orbits that exist in (1) will exist also in (2), so they are topologically semi-conjugate, but by including the vertical branch in (2) we introduce additional orbits that map onto the vertical branch at the point $x_n = 0$. Similarly, any orbits of (1) will exist also in (3) provided they lie outside the interval $(d_{\mathcal{L}}, d_{\mathcal{R}})$. As $(d_{\mathcal{R}} - d_{\mathcal{L}}) \to 0$ the map (3)

tends to (2), and likewise as $\varepsilon \to 0$ the map (4) tends to (2), so the vertical branch of (2) can be expected to play a similar role in the dynamics as the steep branches of (3) and (4).

Of course we could derive more general maps that (1) is semi-conjugate to, to obtain a more complete classification of their bifurcations. However, as discussed in section 1, our purpose here is to study the hitherto unknown role of hidden orbits in already well understood bifurcation sequences, and such sequences are provided by the specific maps (1)-(4).

To study bifurcations of maps (1)-(4) we will mainly vary the offset $\mu_{\mathcal{R}}$ while keeping all other parameters fixed. Changing the height of the graphs of f by varying $\mu_{\mathcal{R}}$ provides rich bifurcation sequences, with equivalent variations of $\mu_{\mathcal{L}}$ obtained by the mapping $x \mapsto -x$. Even for a piecewise linear map a complete classification of the possible bifurcations is not simple. Different signs of the quantities $a_{\mathcal{R}}$, $a_{\mathcal{L}}$, and $\mu_{\mathcal{L}} - \mu_{\mathcal{R}}$, produce a number of different geometrical classes of the map, and we remark on these classes and the more general classification problem in Appendix A. Our scope here is simply to examine examples of typical bifurcation structures, showing the different ways that hidden orbits populate the bifurcation diagrams of discontinuous maps, introducing unstable branches in just the right way that they become consistent with the more standard sequences in continuous or smooth maps.

2.6. Symbolic notation

To denote periodic orbits of maps (1) and (2), we will use the letters $\mathcal{L}$ and $\mathcal{R}$ to label points in $x < 0$ and $x > 0$, respectively. Additionally, for map (2), we use the letter $\mathcal{C}$ to label the point $x = 0$. Similarly, for map (3), the letters $\mathcal{L}$, $\mathcal{C}$, and $\mathcal{R}$ are used for the partitions $x < d_{\mathcal{L}}$, $d_{\mathcal{L}} < x < d_{\mathcal{R}}$, and $x > d_{\mathcal{R}}$, respectively. For the smooth map (4), as there are no distinct branches, the cycles are identified by referring to the symbolic sequences of the corresponding cycles of the maps (1)-(3). A periodic orbit is denoted by $\mathcal{O}$ with a subscript given by the symbolic sequence labeling the regions visited by iterates. So for example, $\mathcal{O}_c$ refers to a fixed point on the vertical branch at $x = 0$ in maps (1), (2), and to a fixed point on the steep branch close to $x = 0$ in maps (3), (4). Similarly, $\mathcal{O}_{\mathcal{LR}}$ is a 2-cycle with one point on the left and one point on the right.

For unambiguity of the notation, we number the points of a cycle according to the associated symbolic sequence, so, for example, the points $x_0^{\mathcal{LR}}$, $x_1^{\mathcal{LR}}$ of a cycle $\mathcal{O}_{\mathcal{LR}}$ are some $x_0^{\mathcal{LR}} \leqslant 0$ and $x_1^{\mathcal{LR}} \geqslant 0$.

3. Hidden orbits

Let us briefly describe hidden orbits, introduced recently in [16], including how to calculate them. We will define these only for the map (2).

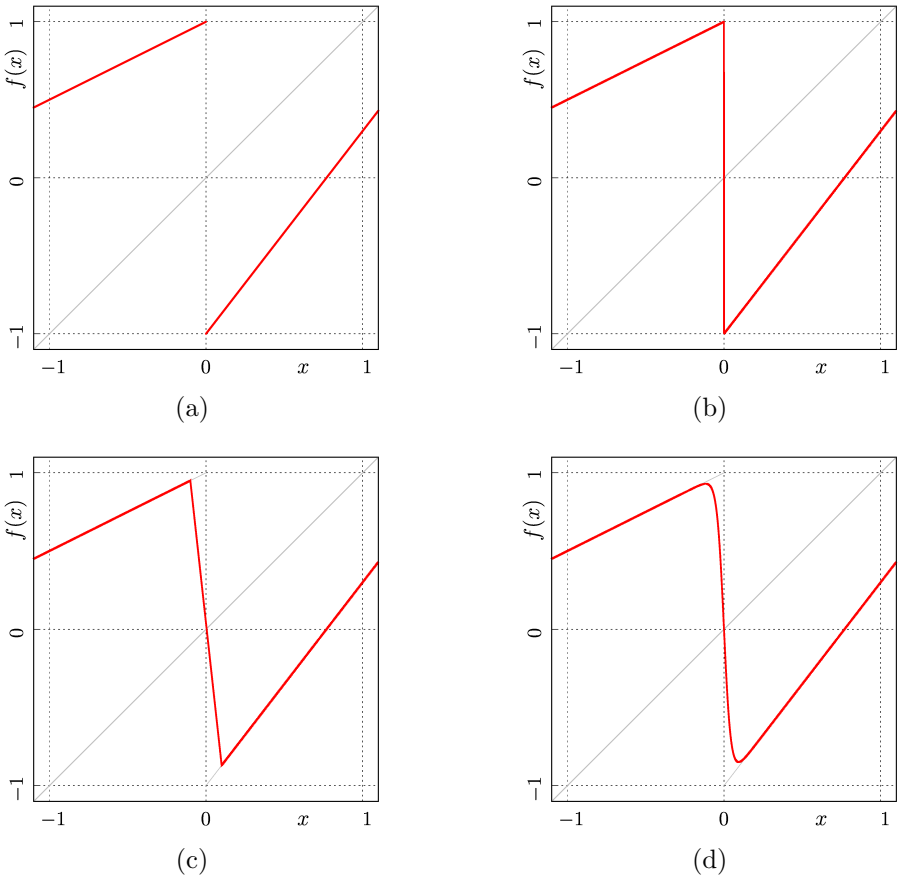

Figure 1. Plots of the four maps: (a) discontinuous map (1); (b) connected map (2); (c) continuous map (3); (d) smooth map (4). Illustrated for parameter values $a_{\mathcal{L}} = 0.5$, $a_{\mathcal{R}} = 1.3$, $\mu_{\mathcal{L}} = 1$, $\mu_{\mathcal{R}} = -1$, $\varepsilon = 0.1$, $d_{\mathcal{L}} = -0.1$, $d_{\mathcal{R}} = 0.1$.

3.1. Definitions

As introduced in [16], a *hidden orbit* is a solution of a dynamical system which includes at least one point lying inside a discontinuity.

In the case of the map (2), an orbit with iterates $\{x_0, x_1, x_2, ...\}$ is hidden if at least one iterate lies at $x_n = 0$, let us say $x_0 = 0$. The first image of $x_0 = 0$ is a point $x_1 = f(0) \in J$. For a given point $x_1 \in J$ the subsequent iterates $x_k = f^{k-1}(x_1)$ with $k > 0$ are then single-valued. Each neighbouring point $x_1 \in J$ generates a distinct orbit $\{0, x_1, f(x_1), f^2(x_1), ...)\}$, which are standard in every respect except they share the common iterate $x_0 = 0$. They behave like any regular orbit, converging to an attractor if one exists, and otherwise diverging.

There are uncountably many of these orbits (the set of all images of the discontinuity), however, if a hidden orbit returns to the same discontinuity then it forms a hidden *periodic* orbit, which we can define as follows.

If a pre-image p of $x_0 = 0$ exists such that $f^k(p) = 0$, and if $p \in J$, then the sequence of

points

$$\begin{aligned} x_0 &= 0, \\ x_1 &= f(0) = p, \\ x_2 &= f^2(0) = f(p), \\ &\vdots \\ x_k &= f^k(p) = 0 \end{aligned} \tag{5}$$

forms a cycle of period $k \geqslant 1$, termed a *hidden periodic orbit* or *hidden cycle* in [16]. By definition, a symbolic sequence associated with a hidden cycle contains at least one letter $\mathcal{C}$.

The simplest hidden cycle of map (2) is the hidden fixed point $\mathcal{O}_c$ located on the vertical branch. Clearly, $\mathcal{O}_c$ exists if $f_{\mathcal{L}}(0)$ and $f_{\mathcal{R}}(0)$ have opposite signs. Further examples of hidden cycles can be found throughout this paper, e.g., in Figs. 4(b), 5(b), and 8(b).

Evidently, every hidden cycle is unstable, as it contains a point at a vertical branch of the function. In a continuous map of the form (3) or (4), that approximates the connected map (2) sufficiently closely, any hidden orbit is replaced by a regular orbit with an iterate on a portion of the map that is very steep, and any hidden cycle is replaced by a repelling cycle.

3.2. Calculation and pre-images

The pre-images of $x_0 = 0$ are points x_{-k} such that $f^k(x_{-k}) = 0$, for $k > 0$, and as with any other point, their existence and uniqueness depends the existence and uniqueness of the inverse f^{-1}.

To calculate the points of a hidden orbit by iterating forward from $x = 0$ one must confront the set-valuedness of $f(0)$. This can be avoided by instead iterating backwards from $x = 0$, using the inverse functions $f_{\mathcal{L}}^{-1}$ and $f_{\mathcal{R}}^{-1}$. For example, to find a hidden k-cycle it is sufficient to assume $x_k = 0$ for some k, and then iterate backwards until finding $x_1 \in J$ and hence $x_0 = 0$. Accordingly, each hidden cycle is given by a sequence of pre-images of zero. In this way, the existence of hidden cycles is closely related to the existence of rank-one pre-images of zero: If there are no such pre-images or if the pre-images exist but are not reachable from the interval J, no hidden cycles can exist.

In addition, this provides us with an immediate clue about border collision bifurcations of hidden orbits. A hidden cycle disappears if its first point $x_1 = f(0) \in J$ collides with a boundary of its definition interval J, i.e., either with $f_{\mathcal{L}}(0)$ or with $f_{\mathcal{R}}(0)$.

3.3. Concatenations

By definition, if the interval J contains more than one pre-image of zero, the map (2) has more than one hidden cycle. In fact, the existence of two distinct pre-images $p_1, p_2 \in J$ implies the existence of infinitely many hidden cycles as follows. Suppose that there exists

a hidden cycle $\mathcal{O}_\sigma$ with $x_0^\sigma = 0$, $x_1^\sigma = p_1$ and a hidden cycle $\mathcal{O}_\varrho$ with $x_0^\varrho = 0$, $x_1^\varrho = p_2$. Then the cycle $\mathcal{O}_{\sigma\varrho}$ formed by their concatenation also exists, as does every irreducible (i.e., corresponding to a prime period of the cycle) concatenation of σ and ϱ, each corresponding to a different cycle.

So the existence of two hidden cycles $\mathcal{O}_{\mathcal{CL}}$ and $\mathcal{O}_{\mathcal{CR}}$ implies the existence of every possibly concatenated cycle $\mathcal{O}_{\mathcal{CLCR}}$, $\mathcal{O}_{(\mathcal{CL})^2\mathcal{CR}}$, $\mathcal{O}_{(\mathcal{CL})^2(\mathcal{CR})^3}$, and so on. Clearly, only irreducible concatenations correspond to distinct hidden cycles (so for example $\mathcal{CLCL}$ corresponds to the same hidden 2-cycle as $\mathcal{CL}$). The family of all finite concatenations of σ and ϱ has a one-to-one mapping to the rational numbers, while all infinite non-repeating concatenations of σ and ϱ have a one-to-one mapping to the irrational numbers, hence the existence of two distinct hidden cycles implies the existence of a countable number of further hidden cycles and an uncountable number of aperiodic hidden orbits.

4. Bifurcations involving finitely many periodic orbits

The simplest bifurcations consist of connections between finitely many branches of attractors or repellers. In a discontinuous map like (1), a single branch can terminate 'in mid air', i.e. without connecting to another branch. This cannot happen in continuous maps like (3) and (4). As we shall see, by rendering a discontinuous map connected as in (2), we obtain the missing connecting branches necessary to interpret such events as standard bifurcations such as, in the example we give below, simple nonsmooth fold and flip bifurcations.

To illustrate this with a general bifurcation scenario, consider the maps (1), (2), (3), and (4) with $-1 < a_\mathcal{L}, a_\mathcal{R} < 0$. The corresponding bifurcation diagrams under variation of the offset $\mu_\mathcal{R}$ are shown in Fig. 2, and we shall describe what happens in these diagrams from right to left, as $\mu_\mathcal{R}$ decreases.

4.1. The discontinuous map

At the parameter value labelled 'A' in Fig. 2(a), the discontinuous map (1) has the stable fixed point

$$\mathcal{O}_\mathcal{R} = \frac{\mu_\mathcal{R}}{1 - a_\mathcal{R}} \tag{6}$$

(see Fig. 3(a)). At $\mu_\mathcal{R} = 0$ this fixed point collides with the border point $x = 0$ and disappears in a border collision bifurcation marked in Fig. 2(a) by $\xi_\mathcal{R}$. Prior to that, a stable 2-cycle

$$\mathcal{O}_{\mathcal{LR}} = \{x_0^{\mathcal{LR}}, x_1^{\mathcal{LR}}\} \quad \text{with} \quad x_0^{\mathcal{LR}} = \frac{a_\mathcal{L}\mu_\mathcal{R} + \mu_\mathcal{L}}{1 - a_\mathcal{L}a_\mathcal{R}}, \quad x_1^{\mathcal{LR}} = \frac{a_\mathcal{R}\mu_\mathcal{L} + \mu_\mathcal{R}}{1 - a_\mathcal{L}a_\mathcal{R}} \tag{7}$$

appears via a border collision bifurcation occurring at the parameter value marked by $\xi_{\mathcal{LR}}$ in Fig. 2(a). This parameter value can easily be calculated from the condition

$$f_\mathcal{R} \circ f_\mathcal{L}(0) = 0 \tag{8}$$

which correspond to $x_0^{\mathcal{LR}} = 0$. Accordingly, in the parameter interval between the border collision bifurcations $\xi_{\mathcal{R}}$ and $\xi_{\mathcal{LR}}$, the map (1) has two coexisting attractors, namely the fixed point $\mathcal{O}_{\mathcal{R}}$ and the 2-cycle $\mathcal{O}_{\mathcal{LR}}$ (see Fig. 3(b)). After $\mathcal{O}_{\mathcal{R}}$ disappears in a border collision bifurcation at $\xi_{\mathcal{R}}$, the 2-cycle $\mathcal{O}_{\mathcal{LR}}$ remains the only attractor (see Fig. 3(c)).

Such sequences of bifurcations are quite standard for discontinuous maps, but two distinctions from continuous maps are worth noting. First, the only orbits involved in the border collision bifurcation are the fixed point and the 2-cycle, and so these appear or disappear without connecting to other fixed points or cycles. This is in contradiction to continuous maps where such bifurcations must involve collisions of at least two such fixed points or cycles. Second, neither the eigenvalue of the fixed point $\lambda(\mathcal{O}_{\mathcal{R}}) = a_{\mathcal{R}} < 0$ nor the eigenvalue of the 2-cycle $\lambda(\mathcal{O}_{\mathcal{LR}}) = a_{\mathcal{L}}a_{\mathcal{R}} > 0$ plays any role in determining the course of the bifurcations. This is contrary to smooth maps, where a negative eigenvalue is associated with a flip bifurcation, and a positive eigenvalue to a fold, pitchfork, or transcritical bifurcation (this is also contrary to piecewise smooth continuous maps, although for such maps the necessary 'eigenvalues' are harder to define due to lack of differentiability, see e.g. [10]).

4.2. The connected map

The connected map (2) has all of the same orbits as the discontinuous map (1), plus a number of hidden orbits in addition, that fundamentally alter the bifurcation's appearance and interpretation.

Take first the bifurcation at $\mu_{\mathcal{R}} = \varphi_{\mathcal{LR}}$ in Fig. 4(b). Not only does the stable 2-cycle $\mathcal{O}_{\mathcal{LR}}$ appear, but also an unstable hidden 2-cycle

$$\mathcal{O}_{\mathcal{CR}} = \{x_0^{\mathcal{CR}}, x_1^{\mathcal{CR}}\} \quad \text{with} \quad x_0^{\mathcal{CR}} = 0, \quad x_1^{\mathcal{CR}} = f_{\mathcal{R}}^{-1}(0) = -\frac{\mu_{\mathcal{R}}}{a_{\mathcal{R}}} \,. \tag{9}$$

It can be easily be seen that these cycles coincide at the bifurcation, since the border collision condition $x_0^{\mathcal{LR}} = 0$ implies at $\mu_{\mathcal{R}} = \varphi_{\mathcal{LR}}$ that $x_0^{\mathcal{LR}} = x_0^{\mathcal{CR}}$, while condition (8) implies $f_{\mathcal{L}}(0) = f_{\mathcal{R}}^{-1}(0)$, so that $x_1^{\mathcal{LR}} = x_1^{\mathcal{CR}}$. As $\mu_{\mathcal{R}}$ decreases away from the bifurcation value, the iterates of the cycles move apart as seen in Fig. 2(b), consistent with a *fold* border collision bifurcation occurring in the connected map (2) at $\varphi_{\mathcal{LR}}$.

At the bifurcation where $\mu_{\mathcal{R}} = \psi_{\mathcal{R}}$, one can clearly see in Fig. 2(b) that as $\mu_{\mathcal{R}}$ approaches $\psi_{\mathcal{R}}$ from the right, the point $x_1^{\mathcal{CR}}$ tends to zero, i.e., to the point $x_0^{\mathcal{CR}}$, so that the hidden cycle $\mathcal{O}_{\mathcal{CR}}$ shrinks in size around the fixed point $\mathcal{O}_{\mathcal{R}}$ and at the bifurcation they coincide (since the bifurcation occurs at $\mu_{\mathcal{R}} = 0$ where $x_1^{\mathcal{CR}} = f_{\mathcal{R}}^{-1}(0) = 0 = x_0^{\mathcal{CR}}$). Moreover, for $\mu_{\mathcal{R}} < 0$ the hidden fixed point $\mathcal{O}_r$ appears. Therefore, the bifurcation occurring in the connected map (2) at $\psi_{\mathcal{R}}$ is a *subcritical flip* border collision bifurcation.

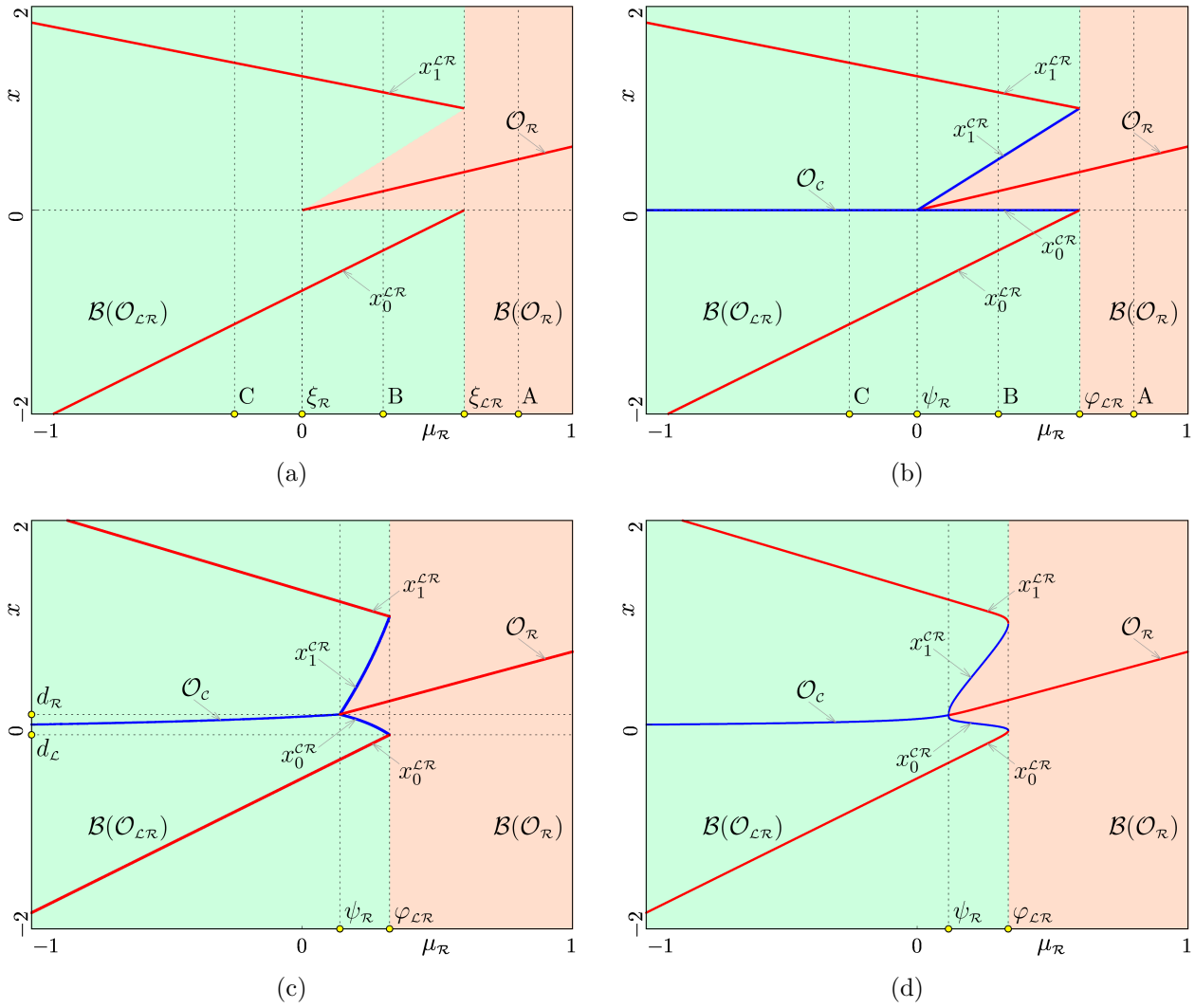

Figure 2. Corresponding bifurcations shown in the: (a) discontinuous map (1); (b) connected map (2); (c) continuous map (3); (d) smooth map (4). Shown for parameter values $a_{\mathcal{L}} = -0.6$, $a_{\mathcal{R}} = -0.4$, $\mu_{\mathcal{L}} = 1$, $\varepsilon = 0.15$, $d_{\mathcal{L}} = -0.1$, $d_{\mathcal{R}} = 0.1$.

4.3. The continuous and the smooth maps

In the continuous map (3), the bifurcation at $\varphi_{\mathcal{LR}}$ is a fold border collision bifurcation occurring at the border point $x = d_{\mathcal{L}}$, and leading to the appearance of the stable cycle $\mathcal{O}_{\mathcal{LR}}$ and the unstable cycle $\mathcal{O}_{\mathcal{CR}}$. At $\psi_{\mathcal{R}}$ the map undergoes a subcritical flip border collision bifurcation occurring at the border point $x = d_{\mathcal{R}}$ at which the stable cycle $\mathcal{O}_{\mathcal{LR}}$ collides with the unstable cycle $\mathcal{O}_{\mathcal{CR}}$ and disappears, and the unstable fixed point $\mathcal{O}_c$ appears. As we let $d_{\mathcal{L}} - d_{\mathcal{R}} \to 0$, Figs. 2(b) and (c) therefore become indistinguishable. In fact, the only difference between the bifurcation structures in maps (2) and (3) (shown in Figs. 2(b) and (c), respectively), is that in map (3) the location of the points $\mathcal{O}_c$ and $x_0^{\mathcal{CR}}$ inside the middle

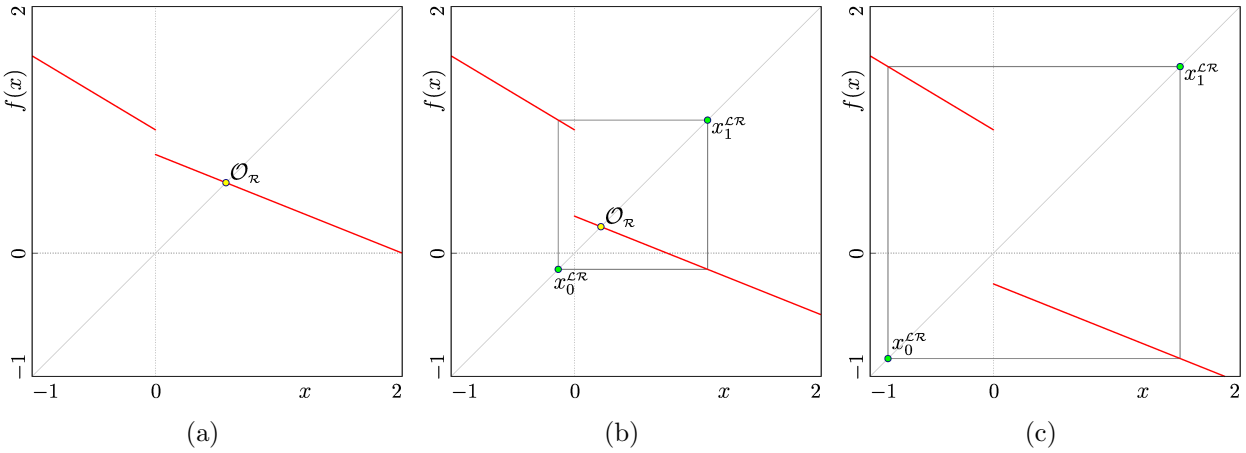

Figure 3. Orbits of the discontinuous map (1) at different places in the bifurcation diagram from Fig. 2(a). In (a) before the border collision bifurcation $\xi_{\mathcal{LR}}$, the fixed point $\mathcal{O}_\mathcal{R}$ is the only attractor. In (b) between the border collision bifurcations $\xi_\mathcal{R}$ and$\xi_{\mathcal{LR}}$, the map has two coexisting attractors, namely the fixed point $\mathcal{O}_\mathcal{R}$ and the 2-cycle $\mathcal{O}_{\mathcal{LR}}$. In (c) after the border collision bifurcation $\xi_\mathcal{R}$, the 2-cycle $\mathcal{O}_{\mathcal{LR}}$ is the only attractor. Shown for parameter values $a_\mathcal{L} = -0.6$, $a_\mathcal{R} = -0.4$, $\mu_\mathcal{L} = 1$, $\mu_\mathcal{R} = 0.8$.

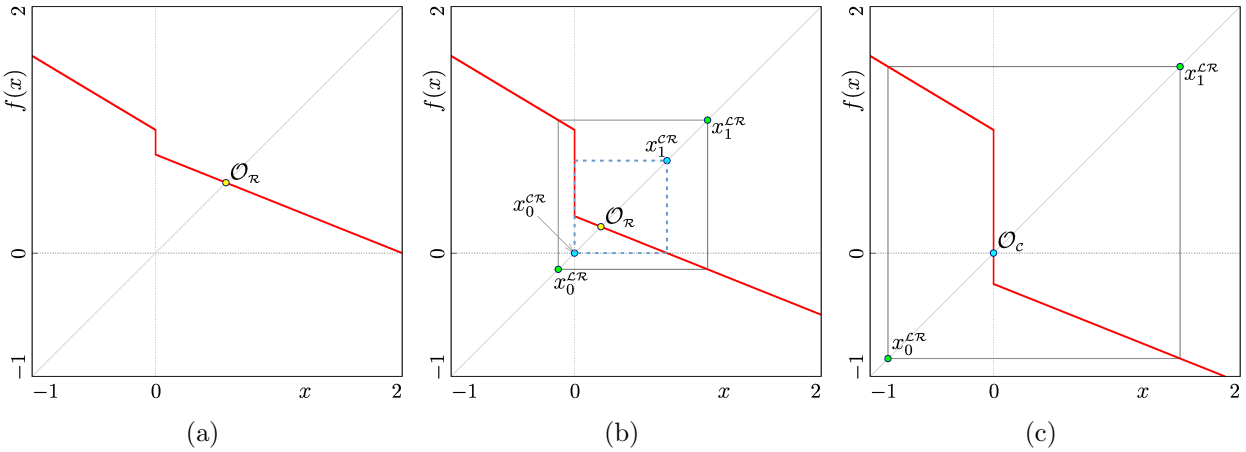

Figure 4. Orbits of the connected map (2) at different places in the bifurcation diagram from Fig. 2(b). In (a) before the border collision bifurcation $\xi_{\mathcal{LR}}$, the fixed point $\mathcal{O}_\mathcal{R}$ is the only attractor. In (b) between the border collision bifurcations $\xi_\mathcal{R}$ and $\xi_{\mathcal{LR}}$, the map has two coexisting attractors, namely the fixed point $\mathcal{O}_\mathcal{R}$ and the 2-cycle $\mathcal{O}_{\mathcal{LR}}$. In (c) after the border collision bifurcation $\xi_\mathcal{R}$, the 2-cycle $\mathcal{O}_{\mathcal{LR}}$ is the only attractor. Shown for the same parameter values as in Fig. 3.

partition $[d_\mathcal{L}, d_\mathcal{R}]$ depends on $\mu_\mathcal{R}$, while in map (2) these points are located at the border point $x = 0$, so that $\mathcal{O}_c$ and $\mathcal{O}_{c\mathcal{R}}$ are hidden orbits.

As is easily seen in Fig. 2(d), in map (4) the bifurcation sequence is similar to the continuous map except that, being smooth, the map exhibits standard fold and subcritical flip bifurcations instead of the corresponding border collision bifurcations. As noted in

section 2.6, the symbolic notation for the cycles used in Fig. 2(d) is merely an echo of the discontinuous maps (2) and (3), as there is no definitive way to partition the smooth map into right, left, and centre regions.

4.4. The different maps compared

Although it now seems trivial for this simple example, we can see that these fold and flip border collision bifurcations in the connected map (2) correspond to, and in fact approximate, fold and flip border collision bifurcations in the continuous map (3), and standard fold and flip bifurcations in the smooth map (4).

However we analyze these maps or describe them symbolically, the structures shown in Figs. 2(b), (c) and (d) are clearly topologically identical, but none is equivalent to Figs. 2(a) where the unstable orbits are 'missing'. For the two simple bifurcations here this distinction is obvious, for more complicated scenarios it will be less so.

Note also that the connected map (2) preserves the relation between the signs of the eigenvalues of the cycles and the bifurcations these cycles undergo in the smooth map (4). Indeed, the fixed point $\mathcal{O}_{\mathcal{R}}$ with a negative eigenvalue undergoes a flip bifurcation in map (4), and so it does in map (2). Similarly, the 2-cycles undergoing fold bifurcations in both maps have positive eigenvalues.

One more feature that the connected map (2) captures and the disconnected map (1) does not is clearly visible in the interval of bistability. In map (1), the basins of attraction of the fixed point $\mathcal{B}(\mathcal{O}_{\mathcal{R}})$ and of the 2-cycle $\mathcal{B}(\mathcal{O}_{\mathcal{LR}})$ are separated from each other by the point of discontinuity and its rank-one pre-image (see Fig. 2(a)). This is a standard situation for discontinuous maps, as described, for example, in [11], where it is stated that in continuous 1D maps, the immediate basin of an attracting fixed point can be confined by two repelling fixed points, by a repelling fixed point and its rank-one pre-image, or by the points of a repelling 2-cycle, and in discontinuous 1D maps it can also be confined by a point on a discontinuity and its pre-image or by two points on a discontinuity. While the latter condition is obviously necessary for discontinuous maps, we see it can be completely avoided by adding a connecting vertical branch to the definition of the map (even if this branch does not exist in the modeled system) and by taking into account the hidden orbits appearing by this extension.

Moreover, proceeding in this way one can obtain some additional information. Indeed, it is clear that in a map with two discontinuities the points discontinuity may form the basin boundary but need not do. The conditions under which this happens are not mentioned in [11], but it is now quite obvious that this happens if the corresponding connected map has two hidden fixed points at the corresponding discontinuities. Similarly, the basin in a discontinuous map is confined by a point on a discontinuity and its pre-image if the corresponding connected map has a hidden 2-cycle at the basin boundary.

It can be easily seen in Fig. 2(b) that in map (2) the basins of attraction $\mathcal{B}(\mathcal{O}_\mathcal{R})$ and $\mathcal{B}(\mathcal{O}_{\mathcal{LR}})$ are separated from each other by the points of the hidden 2-cycle $\mathcal{O}_{\mathcal{CR}}$ (which are, in fact, given by the point of discontinuity and its rank-one pre-image). Therefore, the connected map shows the same behaviour as the continuous maps (3) and (4) (see Figs. 2(c) and (d), respectively) for which the basins are also separated by a repelling 2-cycle $\mathcal{O}_{\mathcal{CR}}$ as well.

5. Bifurcations involving infinitely many periodic orbits

In the example discussed above, a just a few branches were missing in the bifurcations occurring in the discontinuous map (1) compared with the bifurcations in the continuous maps (3) and (4). As we have shown, these branches are restored in the connected map (2). In other situations, the difference between the bifurcations in the discontinuous map (1) and the continuous maps (3)-(4) is even stronger, given by an infinite number of orbits, periodic and aperiodic. As we shall see, the connected map (2) is able to restore these orbits as well.

Consider the map (1) with $0 < a_\mathcal{L} < 1$, $a_\mathcal{R} < -1$, $\mu_\mathcal{L} < 0$, and $\mu_\mathcal{R}$ increasing through zero. As in the previous section we discuss the resulting bifurcations in the maps (1), (2), (3), (4), in turn.

5.1. The discontinuous map

The bifurcation occurring in the discontinuous map (1) as $\mu_\mathcal{R}$ increases is simple. For all values of $\mu_\mathcal{R}$, the map has an attracting fixed point $\mathcal{O}_\mathcal{L} = \mu_\mathcal{L}/(1-a_\mathcal{L})$ in the left partition. For negative values of $\mu_\mathcal{R}$, this fixed point is globally attracting, the map has no other invariant sets. As $\mu_\mathcal{R}$ increases through zero, the fixed point

$$\mathcal{O}_\mathcal{R} = \frac{\mu_\mathcal{R}}{1 - a_\mathcal{R}} \tag{10}$$

appears in the right partition, however, as $a_\mathcal{R} < -1$, it is repelling and so every orbit except for this fixed point still converges to $\mathcal{O}_\mathcal{L}$ (see Fig. 6(a)). The oddity of this bifurcation is that $\mathcal{O}_\mathcal{R}$ appears at $\mu_\mathcal{R} = 0$ with no other fixed points appearing or disappearing to accompany it.

5.2. The connected map

In the connected map (2), the bifurcation is more rich and more standard at the same time. It is immediately clear from Fig. 5(a) that the fixed point $\mathcal{O}_\mathcal{R}$ appears simultaneously with the hidden fixed point $\mathcal{O}_\mathcal{C}$, as would be expected of a fold bifurcation in a continuous map. However, an infinite number of repelling cycles also appear. For $\mu_\mathcal{R} > 0$ there exists the rank-one pre-image of zero, $f_\mathcal{R}^{-1}(0)$, and since $a_\mathcal{R} < -1$, there also exists the infinite sequence of further pre-images $f_\mathcal{R}^{-k}(0)$, $k \geqslant 2$ (see Fig. 5(b)) given by

$$f_\mathcal{R}^{-k}(0) = \frac{\mu_\mathcal{R}}{1 - a_\mathcal{R}} \cdot \frac{a_\mathcal{R}^k - 1}{a_\mathcal{R}^k}. \tag{11}$$

It follows from (10) and (11) that that all these pre-images belong to the interval $(0, \mu_{\mathcal{R}}) \subset J$, and in backward time the sequence of pre-images converges towards the repelling fixed point $\mathcal{O}_{\mathcal{R}}$. Accordingly, for each $k \geqslant 1$ there exists the hidden $(k+1)$-cycle

$$\mathcal{O}_{\mathcal{R}^k\mathcal{C}} = \left\{ f_{\mathcal{R}}^{-k}(0), f_{\mathcal{R}}^{-k+1}(0), \ldots, f_{\mathcal{R}}^{-1}(0), 0 \right\}, \tag{12}$$

as illustrated in Fig. 6(b) (see also a few examples in Fig. 5(b)). Together with the hidden fixed point $\mathcal{O}_{\mathcal{C}}$, the union of these cycles forms the family

$$\mathcal{F}_{\mathcal{R}^k\mathcal{C}} = \{\mathcal{O}_\sigma \mid \sigma \in \Sigma_{\mathcal{R}^k\mathcal{C}}\}, \quad \Sigma_{\mathcal{R}^k\mathcal{C}} = \left\{\sigma_k = \mathcal{R}^k\mathcal{C} \mid k \geqslant 0\right\}, \tag{13}$$

It is worth noting that at the bifurcation occurring at $\mu_{\mathcal{R}} = 0$, not only do the cycles belonging to the family $\mathcal{F}_{\mathcal{R}^k\mathcal{C}}$ appear, but also their concatenations, both finite and infinite, as discussed below.

5.3. The continuous and smooth maps

In the continuous map (3), the bifurcation occurs at the value of $\mu_{\mathcal{R}}$ defined by the condition $f_{\mathcal{R}}(d_{\mathcal{R}}) = d_{\mathcal{R}}$, i.e., $\mu_{\mathcal{R}} = d_{\mathcal{R}}(1 - a_{\mathcal{R}})$ (that means, at $\mu_{\mathcal{R}} = 0.25$ in the example shown in Fig. 6(c)). It can be easily shown that in map (3) not only the repelling fixed point $\mathcal{O}_{\mathcal{R}}$ appears in the right partitions (coinciding with the corresponding fixed points of the discontinuous maps (2) and (1)), but also the repelling fixed point

$$\mathcal{O}_{\mathcal{C}} = \frac{d_{\mathcal{L}} d_{\mathcal{R}}(a_{\mathcal{L}} - a_{\mathcal{R}}) + \mu_{\mathcal{L}} d_{\mathcal{R}} - \mu_{\mathcal{R}} d_{\mathcal{L}}}{\mu_{\mathcal{L}} - \mu_{\mathcal{R}} - d_{\mathcal{R}}(a_{\mathcal{R}} - 1) + d_{\mathcal{L}}(a_{\mathcal{L}} - 1)} \tag{14}$$

belonging to the middle partition. As expected, for both $d_{\mathcal{L}}$ and $d_{\mathcal{R}}$ tending to zero, the fixed point $\mathcal{O}_{\mathcal{C}}$ of map (3) tends to zero as well, and hence to the hidden fixed point $\mathcal{O}_{\mathcal{C}}$ of map (2). As the map (3) is continuous, this bifurcation is a standard fold border collision bifurcation of the saddle-saddle type, leading to the appearance of two repelling fixed points and a set on which the map is chaotic (a chaotic attractor if there is an invariant absorbing interval after the bifurcation or a chaotic repeller otherwise). Since the values of $a_{\mathcal{L}}$, $a_{\mathcal{R}}$ and $\mu_{\mathcal{L}}$ satisfy the condition $f_{\mathcal{R}}^2(d_{\mathcal{R}}) < \mathcal{O}_c$, the bifurcation does not lead to the appearance of an invariant absorbing interval, so that the map after the bifurcation has a chaotic repeller.

In the smooth map (4), the bifurcation occurs when the function becomes tangent to the diagonal. This is a standard fold (saddle-node) bifurcation leading to the appearance of the attracting fixed point $\mathcal{O}_{\mathcal{R}}$ and the repelling fixed point $\mathcal{O}_{\mathcal{C}}$ (tending for $\varepsilon \to 0$ to the hidden fixed point of the connected map (2)). Then, for increasing $\mu_{\mathcal{R}}$ the attracting fixed point $\mathcal{O}_{\mathcal{R}}$ becomes repelling, the map undergoes the standard period-doubling cascade, followed by the appearance of chaotic attractors (see Fig. 6(d)). At the parameter value where the invariant absorbing interval of the map touches the repelling fixed point $\mathcal{O}_{\mathcal{C}}$, a final bifurcation occurs (indicated by χ in Fig. 6(d)), turning the chaotic attractor into a chaotic repeller.

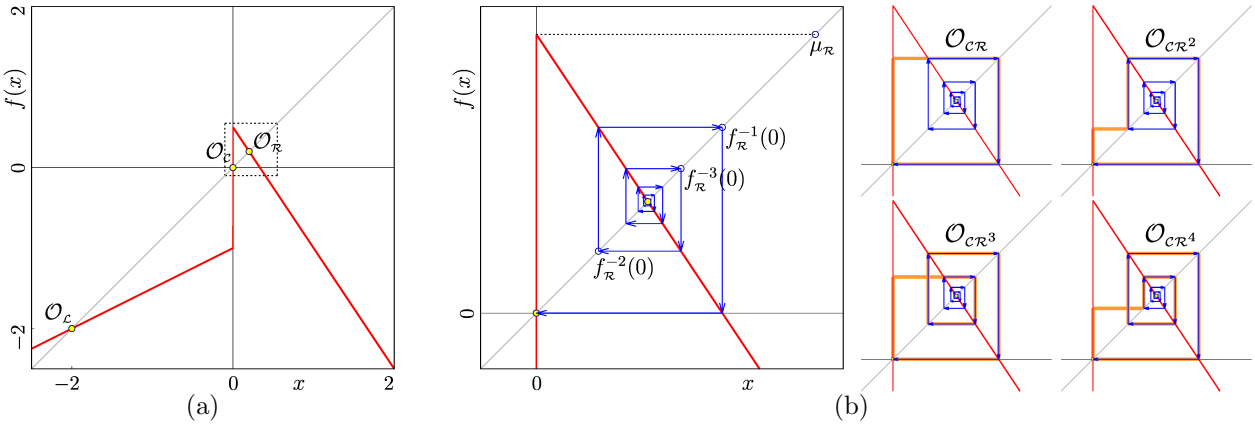

Figure 5. Orbits of the connected map (2). (a) The fold bifurcation creates the pair of fixed points, $\mathcal{O}_{\mathcal{R}}$ and $\mathcal{O}_{\mathcal{C}}$, plus an infinite number of further hidden orbits (cycles and aperiodic orbits). (b) Magnification of the rectangle marked in (a), the rank-1, -2 and -3 pre-images of zero are indicated. Additionally, hidden cycles $\mathcal{O}_{\mathcal{C}\mathcal{R}^k}$, $k = 1, \ldots, 4$ are shown. $a_{\mathcal{L}} = 0.5$, $a_{\mathcal{R}} = -1.5$, $\mu_{\mathcal{L}} = -1$, $\mu_{\mathcal{R}} = 0.5$.

5.4. The different maps compared

As one can see for both the continuous and smooth maps, the bifurcations lead eventually to the appearance of chaotic repellers (immediately after the saddle-saddle bifurcation in map (3) or after all the flip and fold bifurcations following the initial saddle-node bifurcation in map (4)). As the connected map (2) represents a limiting case for maps (3) and (4), for $d_{\mathcal{L}}, d_{\mathcal{R}} \to 0$ the fold bifurcation value ψ in map (3) tends do zero, and for $\varepsilon \to 0$ both bifurcation values ψ and χ tend to zero as well. However, a chaotic repeller forms a Cantor set and consists of a countable number of repelling cycles as well as an uncountable number of repelling aperiodic orbits. As the connected map (2) represents a limiting case for maps (3) and (4) and can be seen as an approximation for these maps, it is a natural question how this approximation maintains these orbits. In fact, this question is quite natural since the family $\mathcal{F}_{\mathcal{R}^k\mathcal{C}}$ we have identified so far is countable.

Perhaps the most non-trivial property of hidden orbits is that they can be concatenated so that the existence of two distinct hidden orbits $\mathcal{O}_{\mathcal{C}\sigma}$ and $\mathcal{O}_{\mathcal{C}\rho}$ implies the the existence of the hidden orbit $\mathcal{O}_{\mathcal{C}\sigma\mathcal{C}\rho}$. The validity and interpretation of such concatenations is not immediately obvious, but as we shall see all concatenations should be considered as valid orbits, as they are needed to make the results for map (2) matching the corresponding results for maps (3) and (4).

As already mentioned, the fixed points $\mathcal{O}_{\mathcal{R}}$ and $\mathcal{O}_{\mathcal{C}}$ of maps (3) and (4) are preserved in their approximation by the connected map (2), the former one as a regular fixed point and the latter one as a hidden fixed point. The 2-cycle $\mathcal{O}_{\mathcal{C}\mathcal{R}}$ belongs to the family $\mathcal{F}_{\mathcal{R}^k\mathcal{C}}$, as well as one of the 3-cycles, namely $\mathcal{O}_{\mathcal{C}\mathcal{R}^2}$. However, the other 3-cycle, i.e., $\mathcal{O}_{\mathcal{C}^2\mathcal{R}}$, does not belong to $\mathcal{F}_{\mathcal{R}^k\mathcal{C}}$ (in map (4) both cycles appear via a smooth fold bifurcation at the beginning

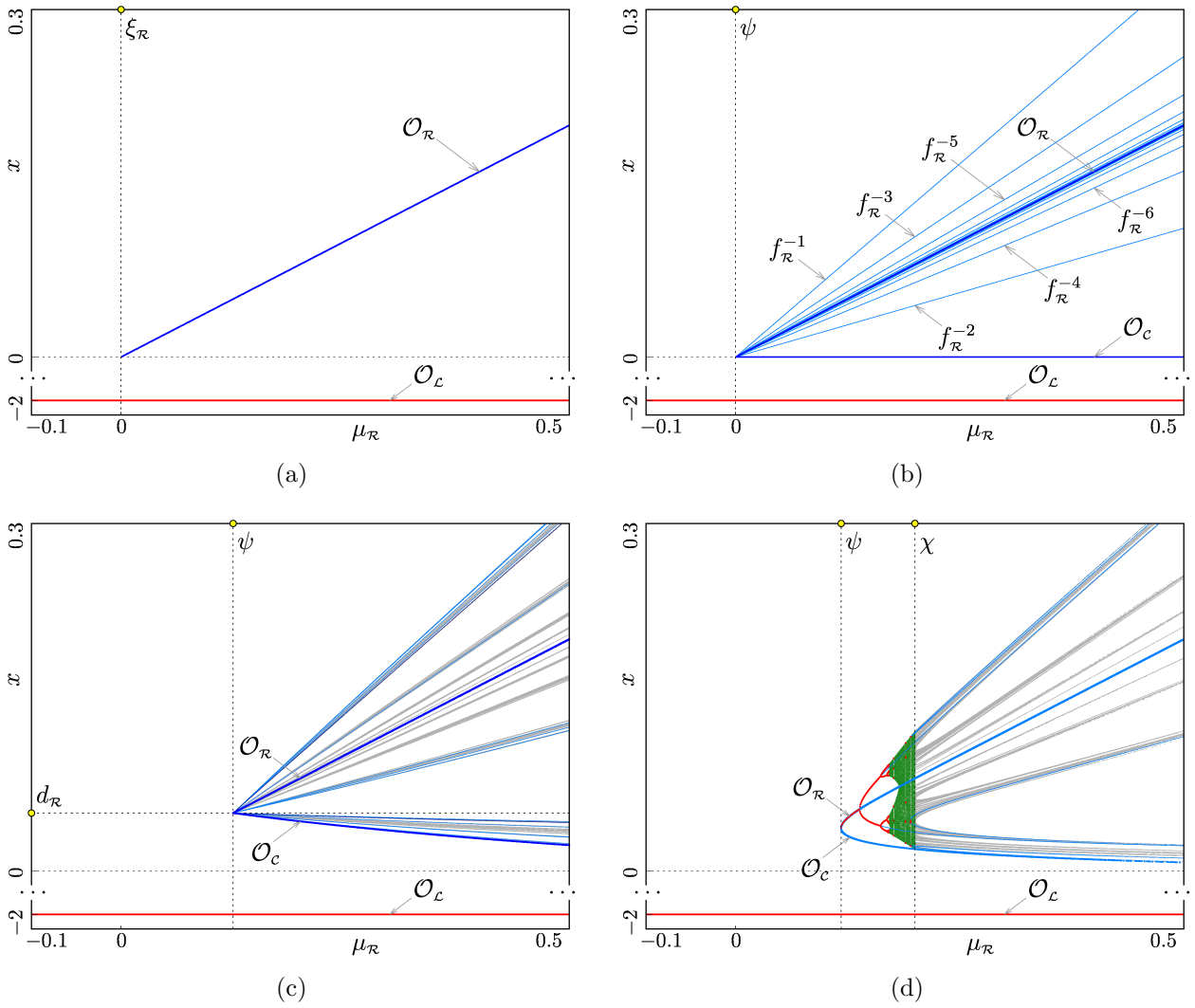

Figure 6. Corresponding bifurcations shown in the: (a) discontinuous map (1); (b) connected map ((2)); (c) continuous map (3); (d) smooth map (4). In (a) the only orbit that appears in the border collision bifurcation $\xi_{\mathcal{R}}$ is the repelling fixed point $\mathcal{O}_{\mathcal{R}}$. In (b) at the fold border collision bifurcation ψ, the usual fixed point $\mathcal{O}_{\mathcal{R}}$ appears (identical with the fixed point $\mathcal{O}_{\mathcal{R}}$ in (a)), as well as the hidden fixed point $\mathcal{O}_{\mathcal{C}}$, a countable number of hidden cycles and an uncountable number of hidden aperiodic orbits. All hidden orbits consist of the point zero and its pre-images $f_{\mathcal{R}}^{-k}$ (marked for $k = 1, \ldots, 6$). In (c) at the fold border collision bifurcation ψ, a chaotic repeller appears, whose points are in a 1 to 1 correspondence with the points of the orbits (hidden or not) appearing in (b). In (d) at the fold border collision bifurcation ψ, a pair of fixed points appear, the stable $\mathcal{O}_{\mathcal{R}}$ and the unstable $\mathcal{O}_{\mathcal{C}}$. The stable fixed point becomes unstable in the usual logistic map scenario, and the eventually appearing chaotic attractor turn into chaotic repeller at the final bifurcation marked by χ. After the final bifurcation, there is a 1 to 1 correspondence between the orbits of maps with the points of orbits (hidden or not) appearing in (b). Stable fixed points and cycles are shown in red, unstable in blue for periods $p = 1, 2, 3, 4$ and in gray for $p = 5, 6, 7, 8$. Shown for parameter $a_{\mathcal{L}} = 0.6$, $a_{\mathcal{R}} = -1.6$, $\mu_{\mathcal{L}} = -1$, $\varepsilon = 0.1$, $d_{\mathcal{L}} = -0.1$, $d_{\mathcal{R}} = 0.1$.

of the period-3 window, while in map (3) they appear at the same fold border collision bifurcation as the fixed points $\mathcal{O}_{\mathcal{R}}$ and $\mathcal{O}_{\mathcal{C}}$). Instead, the associated symbolic sequence is a concatenation of two sequences belonging to $\Sigma_{\mathcal{R}^k\mathcal{C}}$, namely σ_0 and σ_1. In this sense, one can say that the hidden 3-cycle $\mathcal{O}_{\mathcal{C}^2\mathcal{R}} \equiv \mathcal{O}_{\sigma_0\sigma_1}$ appearing at the fold bifurcation in map (2) can be seen as a concatenation of $\mathcal{O}_{\mathcal{C}}$ and $\mathcal{O}_{\mathcal{C}\mathcal{R}}$. Similarly, among the hidden 4-cycles appearing at this bifurcation, the cycle $\mathcal{O}_{\mathcal{C}\mathcal{R}^3}$ belongs to the family $\mathcal{F}_{\mathcal{R}^k\mathcal{C}}$, and two other 4-cycles $\mathcal{O}_{\mathcal{C}^2\mathcal{R}^2}$ and $\mathcal{O}_{\mathcal{C}^3\mathcal{R}}$ result from the corresponding concatenations, namely $\mathcal{O}_{\mathcal{C}^2\mathcal{R}^2} \equiv \mathcal{O}_{\sigma_0\sigma_2}$ and $\mathcal{O}_{\mathcal{C}^3\mathcal{R}} \equiv \mathcal{O}_{\sigma_0\sigma_0\sigma_1}$, respectively. Proceeding in this way, one can easily show that for each repelling cycle belonging to the chaotic repeller in maps (3) and (4) the corresponding symbolic sequence either belongs to the family $\Sigma_{\mathcal{R}^k\mathcal{C}}$ or can be obtained by a finite concatenation of the sequences belonging to this family. Moreover, there is a one-to-one correspondence between the set of these cycles and the set of hidden cycles of map (2). As for the uncountable set of repelling aperiodic orbits belonging to the chaotic repeller in maps (3) and (4), the corresponding hidden aperiodic orbits in map (2) result from infinite concatenations of hidden cycles belonging to the family $\mathcal{F}_{\mathcal{R}^k\mathcal{C}}$.

To summarize, this example shows how a fold bifurcation in the connected map (2) bridges the gap between maps (1) and (3)-(4) by capturing the unstable orbits of Figs. 5(c-d) that are missing from (a) as hidden orbits, resulting in topologically standard structure.

6. Bifurcations at accumulation points

Finally we consider accumulation points, where a cascade of bifurcation curves accumulate towards a particular parameter value. Here the hidden orbits play a role in the organisation of the whole cascade, and not just a single bifurcation event. Such points were perhaps first observed in [22] and various examples can be found in [11]. In section 4 and 5, hidden orbits provided a link between the discontinuous map and well understood bifurcation structures in continuous or smooth maps. In this section, the corresponding cascades in the continuous or smooth maps have not previously been studied to our knowledge, and hidden orbits not only add structure to the bifurcations of the discontinuous map, but provide an approximation of similar bifurcations in the continuous or smooth maps.

As before let us take the map (1), now with $0 < a_{\mathcal{L}}, a_{\mathcal{R}} < 1$, $\mu_{\mathcal{L}} > 0$, and again, considering $\mu_{\mathcal{R}}$ increasing through zero, let us consider the bifurcations exhibited by the discontinuous, connected, continuous, and smooth maps in turn.

We will focus on the important phenomenon of *period adding* sequences in the discontinuous map. The discontinuous map (1) in this case shows the well-known period-adding structure, and we will show that hidden orbits play a role in this structure not only at the bifurcation at $\mu_{\mathcal{R}} = 0$, but throughout the period adding sequence.

In order to present this structure in its complete form, below we discuss dynamics of maps (1)-(4) under a simultaneous variation of $\mu_{\mathcal{R}}$ and $\mu_{\mathcal{L}}$, fixing $\mu_{\mathcal{L}} = \mu_{\mathcal{R}} + 2$ without loss of

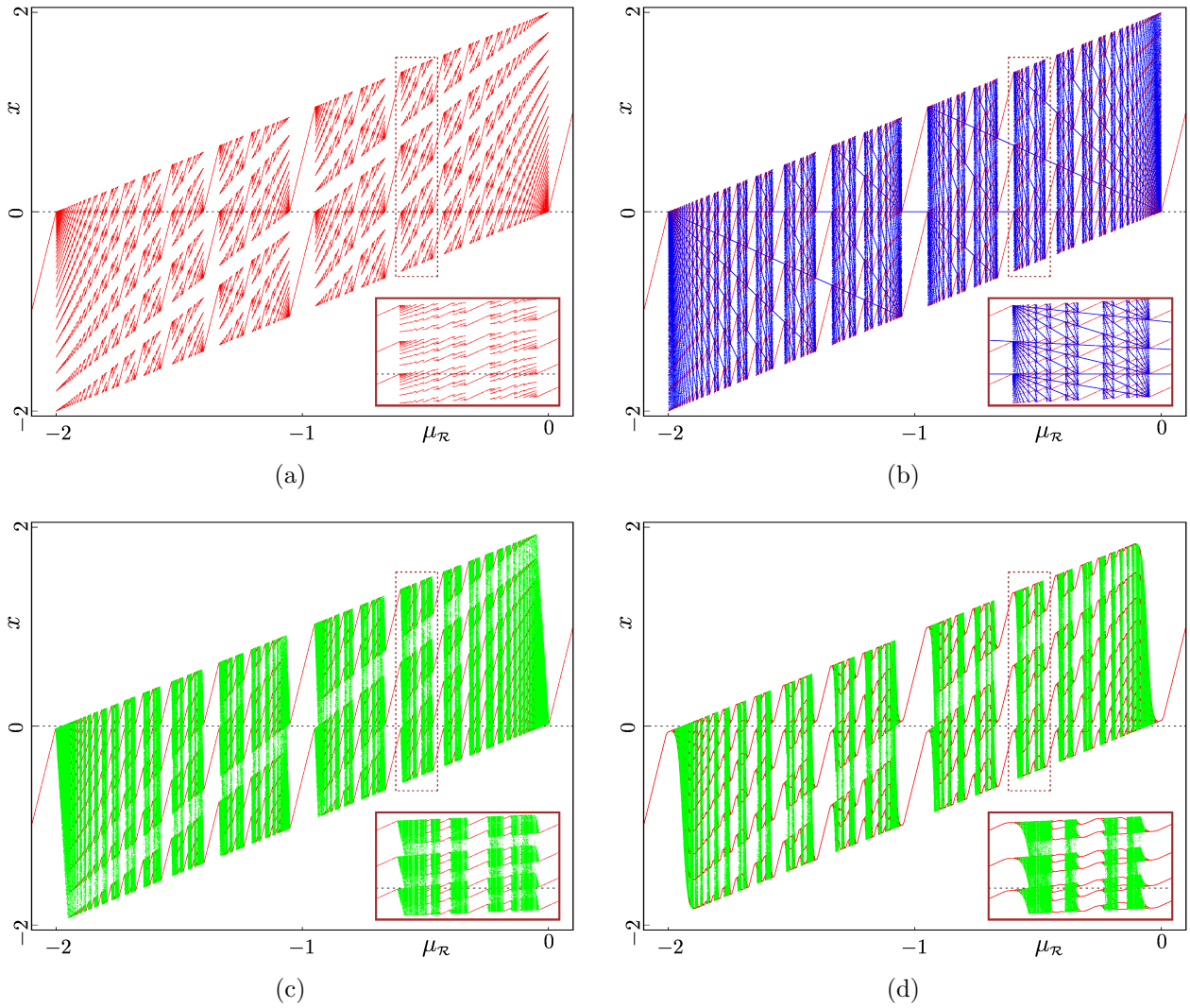

Figure 7. Corresponding bifurcations shown in the: (a) discontinuous map (1); (b) connected map (2); (c) continuous map (3); (d) smooth map (4). Stable cycles are shown in red, hidden ones in blue, chaotic attractors in green. The insets show magnifications of the rectangular regions indicated. Shown for parameter values $a_{\mathcal{L}} = a_{\mathcal{R}} = 0.9$, $\mu_{\mathcal{L}} = \mu_{\mathcal{R}} + 2$, $\varepsilon = 0.1$, $d_{\mathcal{L}} = -0.025$, $d_{\mathcal{R}} = 0.025$.

generality. (This particular coupling of parameters $\mu_{\mathcal{L}}$ and $\mu_{\mathcal{R}}$ makes the system for $a_{\mathcal{L}} = a_{\mathcal{R}}$ identical with the $\Sigma - \Delta$ modulator model introduced in [23] and investigated extensively in [15, 11].) Note that this choice of parameters does not change the bifurcation occurring at $\mu_{\mathcal{R}} = 0$ (since for parameter values close to this bifurcation, it holds that $\mu_{\mathcal{R}} \ll \mu_{\mathcal{L}}$) but does conveniently provide a complete bifurcation sequence, being sandwiched between the stability domain of two stable fixed points.

6.1. The discontinuous map: Standard period adding

An example of the period adding structure in the discontinuous map (1) is shown in Fig. 7(a). Let us briefly recall what is known about the organizing principles of this structure. It is easy to see that for $\mu_{\mathcal{R}} > 0$ the map has a stable and globally attracting fixed point $\mathcal{O}_{\mathcal{R}}$. As $\mu_{\mathcal{R}}$ is varied from positive to negative values, this fixed point disappears in a border collision bifurcation, and a period adding sequence appears for which $\mu_{\mathcal{R}} = 0$ is an accumulation point.

The description of this structure goes back to the pioneering works by Leonov ([22, 24, 25]), who used a recursive approach following so-called complexity levels. According to this approach, the two fixed points $\mathcal{O}_{\mathcal{L}}$ and $\mathcal{O}_{\mathcal{R}}$ form the complexity level zero, and between the parameter regions associated with each two consecutive cycles $\mathcal{O}_\sigma$ and $\mathcal{O}_\varrho$ of complexity level m, there are two infinite families of regions associated with cycles $\mathcal{O}_{\sigma^k\rho}$ and $\mathcal{O}_{\sigma\rho^k}$, $k \geqslant 1$. It is worth noting that for $k \to \infty$ the sequence of regions associated with the cycles $\mathcal{O}_{\sigma^k\rho}$ converges towards a boundary of the region associated with $\mathcal{O}_\sigma$, and the infinite sequence of regions associated with $\mathcal{O}_{\sigma\rho^k}$ converges towards a boundary of the region associated with $\mathcal{O}_\varrho$ (see [11] for details). It follows that for each $m \geqslant 1$ there are 2^m families of cycles of complexity level m. For example, the cycles of complexity level $m = 1$ are the well-known basic (also called maximal, or principle) cycles $\mathcal{O}_{\mathcal{L}^k\mathcal{R}}$ and $\mathcal{O}_{\mathcal{L}\mathcal{R}^k}$, $k \geqslant 1$, the cycles of complexity level two are $\mathcal{O}_{(\mathcal{L}^{k_1+1}\mathcal{R})^{k_2}\mathcal{L}^{k_1}\mathcal{R}}$, $\mathcal{O}_{\mathcal{L}^{k_1+1}\mathcal{R}(\mathcal{L}^{k_1}\mathcal{R})^{k_2}}$, $\mathcal{O}_{(\mathcal{L}\mathcal{R}^{k_1})^{k_2}\mathcal{L}\mathcal{R}^{k_1+1}}$, and $\mathcal{O}_{\mathcal{L}\mathcal{R}^{k_1}(\mathcal{L}\mathcal{R}^{k_1+1})^{k_2}}$, $k_1, k_2 \geqslant 1$, and so on. For this reason, in the open parameter interval $\mu_{\mathcal{R}} \in (-\varepsilon, 0)$ with an arbitrary small $\varepsilon > 0$ there exists an infinite number of parameter intervals associated with basic cycles $\mathcal{O}_{\mathcal{L}\mathcal{R}^k}$, $k \geqslant k_0(\varepsilon)$, $k_0(\varepsilon)$ increasing with $\varepsilon \to 0$, as well as a countable set of intervals associated with cycles of complexity levels higher than one, and also an uncountable set of singular parameter values associated with Cantor set attractors (for details we refer to [11]). For each of the cycles, the corresponding parameter interval is confined by the border collision bifurcations, at which the cycle collides with the border $x = 0$ and disappears. Recall that the points of the cycles colliding with the border are referred to as colliding points and the corresponding letters in the symbolic sequences as colliding letters. As usual, below the colliding letters are underlined, so that, for example, the symbolic sequences $\underline{\mathcal{L}}\mathcal{R}\mathcal{R}\mathcal{R}\underline{\mathcal{R}}$ and $\mathcal{L}\mathcal{R}\underline{\mathcal{L}}\mathcal{R}\underline{\mathcal{R}}$ imply that the basic 5-cycle $\mathcal{O}_{\mathcal{L}\mathcal{R}^4}$ collides with the border by the first and the last points, while the 5-cycle $\mathcal{O}_{\mathcal{L}\mathcal{R}\mathcal{L}\mathcal{R}^2}$ of complexity level two collides by the third and the last points, respectively.

6.2. The connected map: Augmented period adding

In the discontinuous map (1), the period adding structure does not involve any repelling cycles, only attracting cycles and Cantor set attractors. In the connected map (1), all these attracting cycles and Cantor set attractors are preserved, but in addition the map has an infinite number of hidden orbits, which leads to a complex augmented period adding structure

that relates closely to continuous maps. Below we describe this structure in detail. In (i), we first identify the hidden orbits appearing at one particular border collision bifurcation in this structure. In (ii), we briefly recall some basic facts about parent-child relations in Farey trees, then we use these to identify the hidden orbits appearing at other bifurcations in the augmented period adding structure, based on the connection to parents in (iii), and the connection to children in (iv).

(i) The hidden orbits appearing at the border collision bifurcation of $\mathcal{O}_\mathcal{R}$

In map (2), the period adding structure is supplemented by hidden orbits, as shown in Fig. 7(b). For $\mu_\mathcal{R} > 0$ no hidden cycles exist, although the map has a pre-image $f_\mathcal{L}^{-1}(0)$, and in fact, an infinite sequence of pre-images $f_\mathcal{L}^{-k}(0)$, $k \geqslant 1$. However, as $f_\mathcal{L}^{-k}(0) < 0$ for all k and the values of $f(0)$ are positive, i.e., $f_\mathcal{L}^{-k}(0) \notin J$, no orbit started at zero or at any of its pre-images can return to zero. Still, it is not true that no hidden orbits exist in this case. In fact, there are an uncountable number of distinct hidden orbits, starting at zero or any of its pre-images under $f_\mathcal{L}^{-1}$. Although there exist only a countable set of initial values for these orbits, once an orbit arrives at zero, it can take any value from the interval $[\mu_\mathcal{R}, \mu_\mathcal{L}]$ (i.e., an uncountable set) and then the forward iterations of this value will be performed by $f_\mathcal{R}$. Clearly all these orbits converge to the stable fixed point $\mathcal{O}_\mathcal{R}$. Nevertheless, their existence is a difference between the connected map (2) and discontinuous map (1).

As $\mu_\mathcal{R}$ passes through zero, the pre-image $f_\mathcal{R}^{-1}(0)$ appears, as well as the infinite sequence of further pre-images $f_\mathcal{R}^{-k}(0)$, $k \geqslant 1$ (see Fig. 8(a)). Accordingly, at $\mu_\mathcal{R} = 0$ the infinite family of hidden cycles $\mathcal{O}_{\mathcal{CR}^k}$, $k \geqslant 1$, appears, as given by Eq. (12). Note that for each k the cycle $\mathcal{O}_{\mathcal{CR}^k}$ exists not for all values of $\mu_\mathcal{R} < 0$, but only as long as all the involved pre-images of zero are located inside the invariant absorbing interval $[f_\mathcal{R}(0), f_\mathcal{L}(0)] = [\mu_\mathcal{R}, \mu_\mathcal{L}]$. Since the sequence of pre-images $f_\mathcal{R}^{-k}(0)$ of zero is monotonously increasing for increasing k, the condition for a hidden cycle to exist is $f_\mathcal{R}^{-k}(0) < f_\mathcal{L}(0)$ and the bifurcation causing this cycle to disappear occurs when

$$f_\mathcal{R}^{-k}(0) = f_\mathcal{L}(0). \tag{15}$$

It follows from Eqs. (11) and (15) that for each $k \geqslant 1$ the hidden $(k+1)$-cycle $\mathcal{O}_{\mathcal{CR}^k}$ exists in the parameter interval

$$\left[\mu_\mathcal{R}^{(k)}, 0\right) \quad \text{where } \mu_\mathcal{R}^{(k)} = \frac{2(a_\mathcal{R} - 1)}{a_\mathcal{R}^{-k} - a_\mathcal{R}}. \tag{16}$$

The latter equation implies also that $\mu_\mathcal{R}^{(k)} < \mu_\mathcal{R}^{(k+1)}$ for all $k \geqslant 1$ and $\lim_{k\to\infty} \mu_\mathcal{R}^{(k)} = 0$. Therefore, at each fixed $\mu_\mathcal{R}^{(1)} < \mu_\mathcal{R}^* < 0$, a finite number of hidden cycles $\mathcal{O}_{\mathcal{CR}^k}$ exists, with $1 \leqslant k \leqslant k_{\max}$, and $k_{\max}$ depending on $\mu_\mathcal{R}^*$ as determined by the condition

$$\mu_\mathcal{R}^{(k_{\max})} \leqslant \mu_\mathcal{R}^* < \mu_\mathcal{R}^{(k_{\max}+1)}. \tag{17}$$

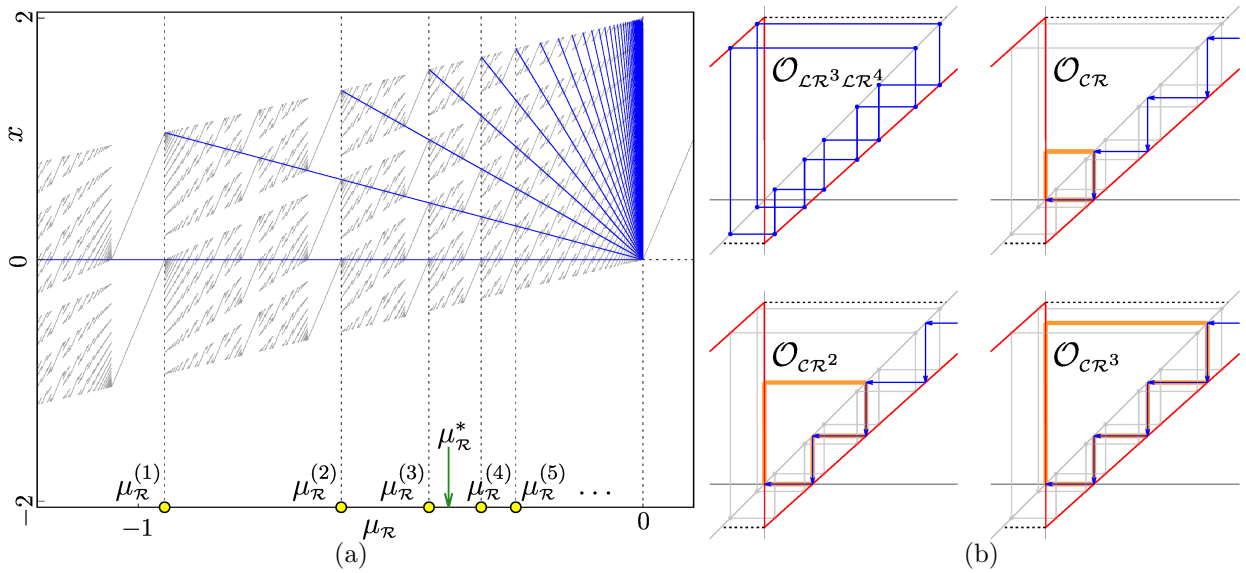

Figure 8. A closer look at the region $\mu_{\mathcal{R}} \in [-1, 0]$ from Fig. 7(b). The magnified bifurcation diagram (a) shows pre-images of zero $f_{\mathcal{R}}^{-k}(0)$, $k = 1, \ldots, 150$, appearing at $\mu_{\mathcal{R}} = 0$ and disappearing at $\mu_{\mathcal{R}}^{(k)}$. For $\mu_{\mathcal{R}} \in [\mu_{\mathcal{R}}^{(k)}, \mu_{\mathcal{R}}^{(k+1)})$, hidden cycles $\mathcal{O}_{\mathcal{CR}}$, ..., $\mathcal{O}_{\mathcal{CR}^k}$ exist. From this, (b) shows the stable cycle $\mathcal{O}_{\mathcal{LR}^3\mathcal{LR}^4}$ and the coexisting hidden cycles $\mathcal{O}_{\mathcal{CR}}$, $\mathcal{O}_{\mathcal{CR}^2}$, $\mathcal{O}_{\mathcal{CR}^3}$ at the parameter value $\mu_{\mathcal{R}}^* = -0.385$ as marked in (a). Shown for parameter values $a_{\mathcal{L}} = a_{\mathcal{R}} = 0.9$, $\mu_{\mathcal{L}} = \mu_{\mathcal{R}} + 2$.

As an example, Fig. 8(b) shows three hidden cycles $\mathcal{O}_{\mathcal{CR}}$, $\mathcal{O}_{\mathcal{CR}^2}$, $\mathcal{O}_{\mathcal{CR}^3}$ coexisting with the stable cycle $\mathcal{O}_{\mathcal{LR}^3\mathcal{LR}^4}$ at the parameter value $\mu_{\mathcal{R}}^* = -0.385$ satisfying $\mu_{\mathcal{R}}^{(3)} \leqslant \mu_{\mathcal{R}}^* < \mu_{\mathcal{R}}^{(4)}$. Note also that these are not the only hidden orbits existing at the considered parameter value. Indeed, the existence of at least two hidden cycles $\mathcal{O}_{\mathcal{C}\sigma}$ and $\mathcal{O}_{\mathcal{C}\varrho}$ implies the existence of a countable number of further hidden cycles and an uncountable number of aperiodic hidden orbits associated with symbolic sequences resulting from finite and infinite concatenations of $\mathcal{C}\sigma$ and $\mathcal{C}\varrho$, respectively. Evidently, all these orbits appear via the bifurcation occurring at $\mu_{\mathcal{R}} = 0$.

(ii). Parent-child relations in Farey trees

So far we have described which hidden orbits (periodic and not) appear at the parameter value $\mu_{\mathcal{R}} = 0$ where the fixed point $\mathcal{O}_{\mathcal{R}}$ undergoes a border collision bifurcation and disappears. To generalize these results and to explain what happens at border collision bifurcations of all other stable cycles forming the period adding structure, we need to recall some basic facts about Farey trees. The classical Farey tree results from a limiting case of Farey sequences. The Farey sequence $\mathcal{F}_m$ of rank $m \geqslant 1$ is defined as a sequence of irreducible fractions with denominators not larger than k, increasing monotonically from $\frac{0}{1}$ to $\frac{1}{1}$. It is known that any three successive fractions $\frac{a_1}{b_1}$ $\frac{a_2}{b_2}$, and $\frac{a_3}{b_3}$ in $\mathcal{F}_m$, $m \geqslant 2$, satisfy the Farey

addition rule $\frac{a_2}{b_2} = \frac{a_1+a_3}{b_1+b_3}$ (this result was proven initially by Haros [26] and independently by Cauchy [27], not by Farey). In this context, the fraction $\frac{a_2}{b_2}$ is called the mediant of $\frac{a_1}{b_1}$ and $\frac{a_3}{b_3}$. Then, the Farey tree is defined as a directed graph consisting of nodes corresponding to fractions in the Farey sequence $\mathcal{F}_\infty = \lim_{m\to\infty} F_m$. For any three successive fractions $\frac{a_1}{b_1}$ $\frac{a_2}{b_2}$, and $\frac{a_3}{b_3}$ in $\mathcal{F}_m$, $m \geqslant 2$, the graph contains the edges from the nodes corresponding to $\frac{a_1}{b_1}$ and $\frac{a_3}{b_3}$ to the node corresponding to their mediant $\frac{a_2}{b_2}$.

A closely related structure, referred to in [11] as the symbolic sequence adding scheme, can be obtained by replacing fractions in a Farey tree by symbolic sequences and the Farey addition by their concatenation. In the simplest case, if the fractions $\frac{0}{1}$ and $\frac{1}{1}$ in the starting nodes of the Farey tree are replaced by the letters $\mathcal{L}$ and $\mathcal{R}$, this structure specifies the symbolic sequences corresponding to cycles in a period adding bifurcation structure between the domains of the fixed points $\mathcal{O}_\mathcal{L}$ and $\mathcal{O}_\mathcal{R}$. If the graph contains edges from the nodes corresponding to symbolic sequences σ and ϱ to a node corresponding $\sigma\varrho$, then σ and ϱ are called the parent sequences of $\sigma\varrho$, and $\sigma\varrho$ the child sequence of σ and ϱ. Basically, for any given sequence ϖ in the symbolic sequence adding scheme, its child-sequences are the sequences belonging to the nodes in the graph to which there is an edge from the node associated with ϖ. It can be shown that each sequence $\sigma\varrho$ with the parent sequences σ and ϱ has two infinite families of child-sequences, namely

$$\ell(\sigma\varrho) = \left\{\sigma(\sigma\varrho)^k \mid k \geqslant 1\right\} \quad \text{and} \quad r(\sigma\varrho) = \left\{(\sigma\varrho)^k\varrho \mid k \geqslant 1\right\}. \tag{18}$$

For example, the sequence $\mathcal{LR}$ associated with a 2-cycle is a child-sequence of the starting sequences $\mathcal{L}$ and $\mathcal{R}$ (the only common child of these sequences). Hence, the families of child-sequences of $\mathcal{LR}$ are

$$\ell(\mathcal{LR}) = \left\{\mathcal{L}(\mathcal{LR})^k \mid k \geqslant 1\right\} \quad \text{and} \quad r(\mathcal{LR}) = \left\{(\mathcal{LR})^k\mathcal{R} \mid k \geqslant 1\right\}. \tag{19}$$

Each of the starting sequences $\mathcal{L}$, and $\mathcal{R}$ has only one family of child-sequences, namely $r(\mathcal{L}) = \left\{\mathcal{L}^k\mathcal{R} \mid k \geqslant 1\right\}$ and $\ell(\mathcal{R}) = \left\{\mathcal{L}\mathcal{R}^k \mid k \geqslant 1\right\}$. The parent-child relationship between symbolic sequences forming a symbolic sequence adding scheme is rarely used in nonlinear dynamics, but turns out to be essential for the description below.

(iii). Connection of a cycle to its parents via hidden cycles

Let us consider now the hidden 2-cycles $\mathcal{O}_{\mathcal{CR}}$ and $\mathcal{O}_{\mathcal{CL}}$ (see Fig. 9(a)). As already mentioned, the cycle $\mathcal{O}_{\mathcal{CR}}$ exists in the parameter interval between $\mu_\mathcal{R} = 0$ (which corresponds to the border collision bifurcation of the fixed point $\mathcal{O}_\mathcal{R}$) and $\mu_\mathcal{R}^{(1)}$ (see definition in (16)). Recall that the latter bifurcation is determined by the condition that the point of the hidden cycle given by $x_1^{\mathcal{CR}} = f_\mathcal{R}^{-1}(0)$ collides with the boundary of the invariant absorbing interval $\mu_\mathcal{L} = f_\mathcal{L}(0)$. Clearly, the condition $f_\mathcal{R}^{-1}(0) = f_\mathcal{L}(0)$ implies $f_\mathcal{R}(f_\mathcal{L}(0)) = 0$, which is the condition causing the non-hidden 2-cycle $\mathcal{O}_{\mathcal{LR}}$ to collide with the border from the left side. In the discontinuous map (1), this bifurcation is associated with the disappearance of a stable 2-cycle $\mathcal{O}_{\mathcal{LR}}$. In

the connected map (2), the colliding point of the 2-cycle moves from a stable to a vertical branch, so that the cycle persists but becomes hidden.

Similarly, for the other hidden 2-cycle $\mathcal{O}_{\mathcal{CL}}$ we find that it exists in the parameter range between the border collision bifurcation of the fixed point $\mathcal{O}_{\mathcal{L}}$ and the other border collision bifurcation 2-cycle $\mathcal{O}_{\mathcal{LR}}$ which is determined by the condition $f_{\mathcal{L}}(f_{\mathcal{R}}(0)) = 0$, or equivalently $f_{\mathcal{L}}^{-1}(0) = f_{\mathcal{R}}(0)$. Accordingly, in the connected map (2) the parameter interval corresponding to the stable 2-cycle $\mathcal{O}_{\mathcal{LR}}$ is surrounded by parameter intervals corresponding to the hidden 2-cycles $\mathcal{O}_{\mathcal{CR}}$ and $\mathcal{O}_{\mathcal{CL}}$. These intervals extend from the border collision bifurcation of $\mathcal{O}_{\mathcal{LR}}$ to the border collision bifurcation of the fixed points associated with the parent sequences of $\mathcal{LR}$, namely $\mathcal{L}$ and $\mathcal{R}$.

To describe the corresponding structure more generally, let us introduce the following notation:

- For a cycle $\mathcal{O}_{\varpi}$, let $\xi_{\varpi}^{\mathcal{L}}$ and $\xi_{\varpi}^{\mathcal{R}}$ be its border collision bifurcations from the left and from the right side, respectively.
- For a symbolic sequence ϖ, let $\varkappa_{\mathcal{L}}(\varpi)$ and $\varkappa_{\mathcal{R}}(\varpi)$ be symbolic sequences resulting from ϖ by replacing its colliding letters $\mathcal{L}$ and $\mathcal{R}$, respectively, by the letter $\mathcal{C}$.

Then, let us now consider a cycle $\mathcal{O}_{\sigma\varrho}$ in the period adding structure of the discontinuous map (1). Let σ and ϱ be the parent sequences of $\sigma\varrho$. Then

(p1) In the connected map (2), at the border collision bifurcations $\xi_{\sigma\varrho}^{\mathcal{L}}$ and $\xi_{\sigma\varrho}^{\mathcal{R}}$ the stable cycle $\mathcal{O}_{\sigma\varrho}$ disappears and the hidden cycles $\mathcal{O}_{\varkappa^{\mathcal{L}}(\sigma\varrho)}$, $\mathcal{O}_{\varkappa^{\mathcal{R}}(\sigma\varrho)}$ appear.

(p2) The hidden cycle $\mathcal{O}_{\varkappa^{\mathcal{L}}(\sigma\varrho)}$ exists in the parameter interval between the border collision bifurcations $\xi_{\sigma\varrho}^{\mathcal{L}}$ and $\xi_{\sigma}^{\mathcal{R}}$. Similarly, the existence interval of the hidden cycle $\mathcal{O}_{\varkappa^{\mathcal{R}}(\sigma\varrho)}$ is confined by the border collision bifurcations $\xi_{\sigma\varrho}^{\mathcal{R}}$ and $\xi_{\varrho}^{\mathcal{L}}$.

Let us illustrate this with a few examples. It is known that if $f_{\mathcal{L}}$ and $f_{\mathcal{R}}$ are increasing functions, the basic cycles $\mathcal{O}_{\mathcal{LR}^k}$, $k \geqslant 1$, collide with the border by the first and the last points. For the 5-cycle $\mathcal{O}_{\mathcal{LR}^4}$, replacing the colliding letter $\mathcal{L}$ and $\mathcal{R}$ by $\mathcal{C}$, we obtain

$$\varkappa^{\mathcal{L}}(\underline{\mathcal{L}}\mathcal{RRRR}) = \mathcal{CRRRR}, \qquad \varkappa^{\mathcal{R}}(\mathcal{LRRR}\underline{\mathcal{R}}) = \mathcal{LRRRC} \equiv \mathcal{CLRRR}. \quad (20)$$

Therefore, the hidden 5-cycles appearing at the border collision bifurcations of $\mathcal{O}_{\mathcal{LR}^4}$ are $\mathcal{O}_{\mathcal{CR}^4}$ and $\mathcal{O}_{\mathcal{CLR}^3}$ (see Fig. 9(b)). Since the points of hidden cycles are given by pre-images of zero, it is easy to see that

$$\begin{aligned}
x_0^{\mathcal{CR}^4} &= 0, & x_0^{\mathcal{CLR}^3} &= 0,\\
x_1^{\mathcal{CR}^4} &= f_{\mathcal{R}}^{-4}(0), & x_1^{\mathcal{CLR}^3} &= f_{\mathcal{L}}^{-1}(f_{\mathcal{R}}^{-3}(0)),\\
x_2^{\mathcal{CR}^4} &= f_{\mathcal{R}}^{-3}(0), & x_2^{\mathcal{CLR}^3} &= f_{\mathcal{R}}^{-3}(0),\\
x_3^{\mathcal{CR}^4} &= f_{\mathcal{R}}^{-2}(0), & x_3^{\mathcal{CLR}^3} &= f_{\mathcal{R}}^{-2}(0),\\
x_4^{\mathcal{CR}^4} &= f_{\mathcal{R}}^{-1}(0), & x_4^{\mathcal{CLR}^3} &= f_{\mathcal{R}}^{-1}(0).
\end{aligned} \quad (21)$$

Taking into account that the hidden cycles exist if $\mu_{\mathcal{R}} < 0$ and the corresponding pre-images of zero are located inside the absorbing interval $I = [\mu_{\mathcal{R}}, \mu_{\mathcal{L}}]$, we conclude that the existence

condition for the cycle $\mathcal{O}_{\mathcal{CR}^4}$ is

$$\mu_{\mathcal{R}} < 0, \quad f_{\mathcal{R}}^{-4}(0) < \mu_{\mathcal{L}} \tag{22}$$

and the existence condition for the cycle $\mathcal{O}_{\mathcal{CLR}^3}$ is

$$\mu_{\mathcal{R}} < f_{\mathcal{L}}^{-1}(f_{\mathcal{R}}^{-3}(0)), \quad f_{\mathcal{R}}^{-3}(0) < \mu_{\mathcal{L}}. \tag{23}$$

Indeed, these conditions follow immediately from the location of the points of the cycles with respect to the boundaries of the absorbing interval I. In particular, for the cycle $\mathcal{O}_{\mathcal{CLR}^3}$ the points located most far away from the border point $x = 0$ and hence most closely to the boundaries of I are $x_1^{\mathcal{CLR}^3}$ and $x_2^{\mathcal{CLR}^3}$, which implies conditions (23).

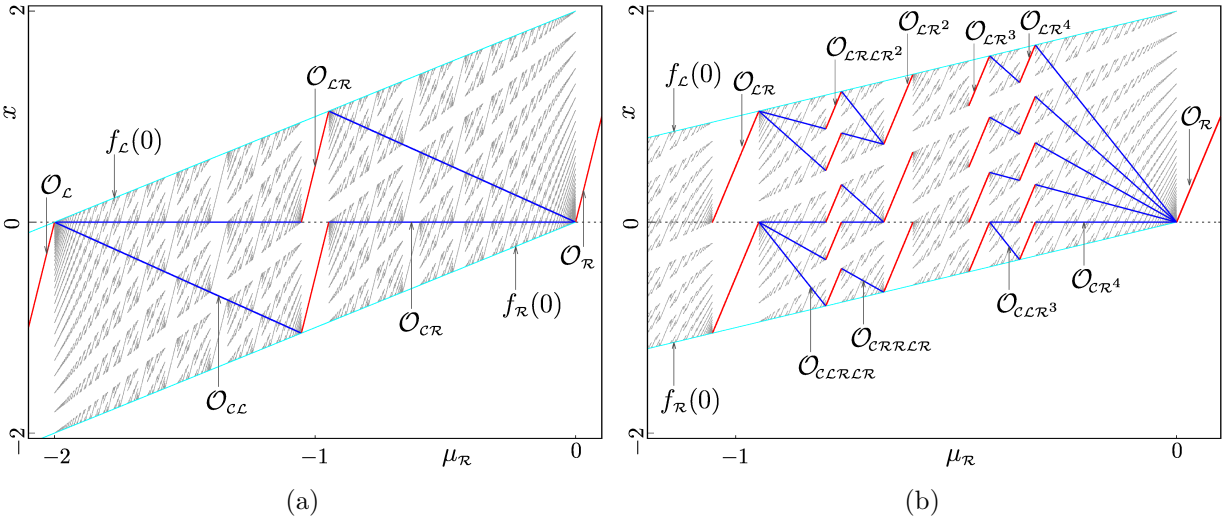

Figure 9. Bifurcation diagrams for the connected map (2) showing: (a) the 2-cycle $\mathcal{O}_{\mathcal{LR}}$, surrounded by the hidden 2-cycles $\mathcal{O}_{\mathcal{CL}}$ and $\mathcal{O}_{\mathcal{CR}}$; (b) the 5-cycles $\mathcal{O}_{\mathcal{LRLR}^2}$ and $\mathcal{O}_{\mathcal{LR}^4}$, surrounded by the hidden 5-cycles $\mathcal{O}_{\mathcal{CLRLR}}$, $\mathcal{O}_{\mathcal{CRRLR}}$, and $\mathcal{O}_{\mathcal{CLR}^3}$, $\mathcal{O}_{\mathcal{CR}^4}$, respectively. Show for parameters $a_{\mathcal{L}} = a_{\mathcal{R}} = 0.9$, $\mu_{\mathcal{L}} = \mu_{\mathcal{R}} + 2$.

Next, recall that the parent sequences of $\mathcal{LR}^4$ are $\mathcal{LR}^3$ and $\mathcal{R}$. It follows from Eq. (22) that the cycle $\mathcal{O}_{\mathcal{CR}^4}$ exists in the parameter interval confined by the parameter values determined by the conditions

$$f_{\mathcal{R}}(0) = 0, \tag{24}$$

$$f_{\mathcal{R}}^{-4}(0) = f_{\mathcal{L}}(0) \quad \Leftrightarrow \quad f_{\mathcal{R}}^{4}(f_{\mathcal{L}}(0)) = 0. \tag{25}$$

As one can see, Eq. (24) corresponds to the border collision bifurcation of $\mathcal{O}_{\mathcal{R}}$ (the fixed point associated with one of the parent sequences of $\mathcal{LR}^4$), while Eq. (25) corresponds to a border collision bifurcation of $\mathcal{O}_{\mathcal{LR}^4}$. Similarly, Eq. (23) implies that the existence interval of the cycle $\mathcal{O}_{\mathcal{CLR}^3}$ is confined by the parameter values determined by the conditions

$$f_{\mathcal{R}}(0) = f_{\mathcal{L}}^{-1}(f_{\mathcal{R}}^{-3}(0)) \quad \Leftrightarrow \quad f_{\mathcal{R}}^{3}(f_{\mathcal{L}}(f_{\mathcal{R}}(0))) = 0, \tag{26}$$

$$f_{\mathcal{L}}(0) = f_{\mathcal{R}}^{-3}(0) \quad \Leftrightarrow \quad f_{\mathcal{R}}^{3}(f_{\mathcal{L}}(0)) = 0. \tag{27}$$

Here, Eq. (26) corresponds to the other border collision bifurcation of $\mathcal{O}_{\mathcal{LR}^4}$, and Eq. (26) to the border collision bifurcation of the 4-cycle $\mathcal{O}_{\mathcal{LR}^3}$ which is associated with the other one of the parent sequences of $\mathcal{LR}^4$. This proves the statements (i) and (ii) in the particular cases $\sigma = \mathcal{LR}^4$.

In addition, Fig. 9(b) illustrates the appearance of hidden cycles at the border collision bifurcations of the 5-cycle $\mathcal{O}_{\mathcal{LRLR}^2}$. Here, it follows from

$$\varkappa^{\mathcal{L}}(\mathcal{LR}\underline{\mathcal{L}}\mathcal{RR}) = \mathcal{LRCRR} \equiv \mathcal{CRRLR} \tag{28}$$

$$\varkappa^{\mathcal{R}}(\mathcal{LRLR}\underline{\mathcal{R}}) = \mathcal{LRLRC} \equiv \mathcal{CLRLR} \tag{29}$$

that the existence interval of the cycle $\mathcal{O}_{\mathcal{LRLR}^2}$ is surrounded by the intervals where the hidden cycles $\mathcal{O}_{\mathcal{CR}^2\mathcal{LR}}$ and $\mathcal{O}_{\mathcal{CLRLR}}$ exist. As one can see in Fig. 9(b), these intervals reach from the parameter values corresponding to the border collision bifurcations of $\mathcal{O}_{\mathcal{LRLR}^2}$ to the border collision bifurcations of $\mathcal{O}_{\mathcal{LR}}$ and $\mathcal{O}_{\mathcal{LR}^2}$ (recall that $\mathcal{LR}$ and $\mathcal{LR}^2$ are the parent sequences of $\mathcal{LRLR}^2$).

The connectedness of the map makes it possible to provide a general proof of (i) and (ii), but this is beyond our scope here. To give a basic idea of the proof, it is simple to show that hidden cycles $\mathcal{O}_{\varkappa^{\mathcal{L}}(\sigma\varrho)}$, $\mathcal{O}_{\varkappa^{\mathcal{R}}(\sigma\varrho)}$ appear at the border collision bifurcations $\xi^{\mathcal{L}}_{\sigma\varrho}$ and $\xi^{\mathcal{R}}_{\sigma\varrho}$, as the connectedness of the map implies that when a fixed point disappears from the $x > 0$ branch of the map, it must either persist as a hidden fixed point or else co-annihilate with one. More involved is to prove that the cycles $\mathcal{O}_{\varkappa^{\mathcal{L}}(\sigma\varrho)}$, $\mathcal{O}_{\varkappa^{\mathcal{R}}(\sigma\varrho)}$ appear at the border collision bifurcations $\xi^{\mathcal{L}}_{\sigma}$ and $\xi^{\mathcal{R}}_{\varrho}$, using the fact that any cycle is a concatenation of its parents, not only in the sense of symbolic sequences, but the geometrical shapes of the parents that are glued together (see Fig. 10(a)), meaning the most outer points of the child cycle are the images of the colliding points which are common for the parent and child cycles.

(iii). Connection of a cycle to its children via hidden cycles

The results obtained so far make it possible to specify the hidden orbits appearing at any border collision bifurcation in the period adding structure in the connected map (2). Indeed, as already mentioned, each sequence $\sigma\varrho$ in the symbolic sequence adding scheme which has the parent sequences σ and ϱ, has two infinite families of child-sequences, namely $\sigma(\sigma\varrho)^k$ and $(\sigma\varrho)^k\varrho$, $k \geqslant 1$. Applying (p1) and (p2) to the corresponding cycles, we conclude that:

(p3) At the border collision bifurcations $\xi^{\mathcal{L}}_{\sigma\varrho}$, in addition to the hidden cycle $\xi^{\mathcal{L}}_{\varkappa^{\mathcal{L}}(\sigma\varrho)}$, also the infinite family of hidden cycles $\mathcal{O}_{\varkappa^{\mathcal{R}}(\sigma(\sigma\varrho)^k)}$ appears. Similarly, at the border collision bifurcations $\xi^{\mathcal{R}}_{\sigma\varrho}$, in addition to the hidden cycle $\xi^{\mathcal{R}}_{\varkappa^{\mathcal{R}}(\sigma\varrho)}$, also the infinite family of hidden cycles $\mathcal{O}_{\varkappa^{\mathcal{L}}((\sigma\varrho)^k\varrho)}$ appears.

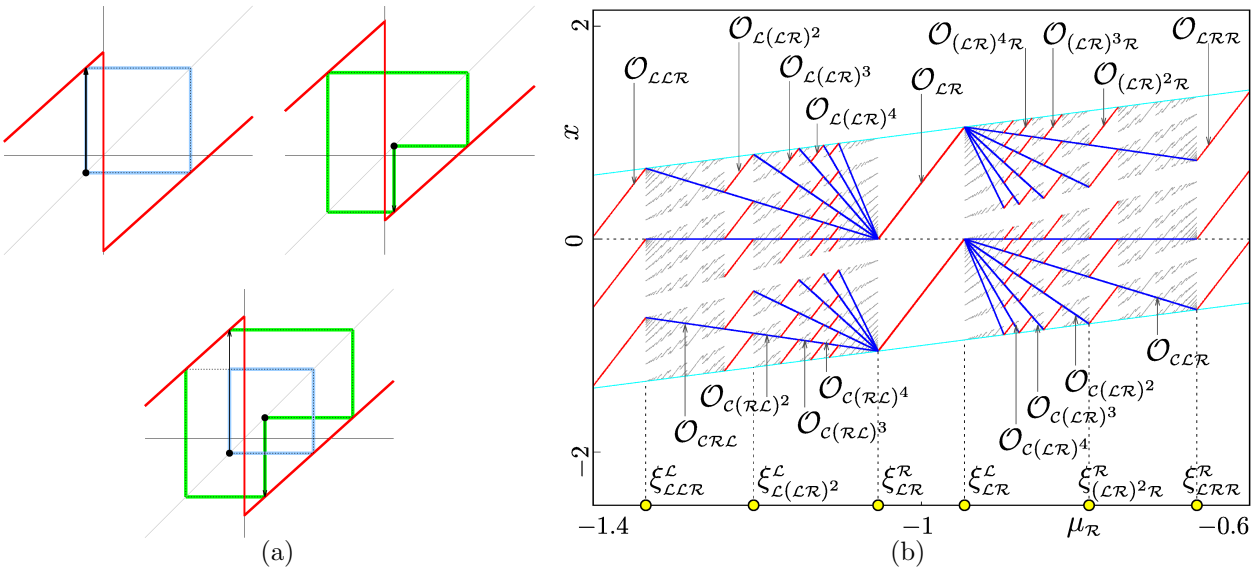

Figure 10. (a) Parent cycles $\mathcal{O}_{\mathcal{LR}}$ (close to the border collision bifurcation $\xi^{\mathcal{L}}_{\mathcal{LR}}$), $\mathcal{O}_{\mathcal{LR}^2}$ (close to $\xi^{\mathcal{R}}_{\mathcal{LR}^2}$), and their child cycle $\mathcal{O}_{\mathcal{LRLR}^2}$. Colliding points are marked. (b) Bifurcations diagram for the connected map (2), showing hidden cycles $\mathcal{O}_{\mathcal{C}(\mathcal{RL})^k}$ and $\mathcal{O}_{\mathcal{C}(\mathcal{LR})^k}$, $k = 1, 2, 3, 4$, appearing at the border collision bifurcations $\xi^{\mathcal{R}}_{\mathcal{LR}}$ and $\xi^{\mathcal{L}}_{\mathcal{LR}}$ of the 2-cycle $\mathcal{O}_{\mathcal{LR}}$. Additionally, the cycles $\mathcal{O}_{\mathcal{L}(\mathcal{LR})^k}$ and $\mathcal{O}_{(\mathcal{LR})^k\mathcal{R}}$, $k = 1, 2, 3, 4$, are shown, associated with the child-sequences of $\mathcal{LR}$. Shown for parameter values $a_{\mathcal{L}} = a_{\mathcal{R}} = 0.9$, $\mu_{\mathcal{L}} = \mu_{\mathcal{R}} + 2$.

(p4) Moreover, at the same bifurcations, all irreducible concatenations of cycles mentioned in (i) and (iii) appear, as well as their concatenations with other hidden cycles existing at these parameter values.

As an example consider the hidden orbits appearing at the border collision bifurcations of the 2-cycle $\mathcal{O}_{\mathcal{LR}}$. As already mentioned, the parent sequences of $\mathcal{LR}$ are $\mathcal{L}$ and $\mathcal{R}$. Using a simple cyclic shift, it can be shown that the families of the child-sequences of $\mathcal{LR}$ given by Eq. (19) can be written as

$$\ell(\mathcal{LR}) = \left\{\mathcal{L}(\mathcal{LR})^k \mid k \geqslant 1\right\} \equiv \left\{\mathcal{RLL}(\mathcal{RL})^{k-1} \mid k \geqslant 1\right\}, \tag{30}$$

$$r(\mathcal{LR}) = \left\{(\mathcal{LR})^k\mathcal{R} \mid k \geqslant 1\right\} \equiv \left\{\mathcal{LRR}(\mathcal{LR})^{k-1} \mid k \geqslant 1\right\}. \tag{31}$$

For $k = 1, \ldots, 4$, these cycles associated with these sequences are shown in Fig. 10(b). Using the algorithm described in [11], it is not difficult to determine the colliding letters in these sequences:

$$\underline{\mathcal{R}}\mathcal{L}\underline{\mathcal{L}}(\mathcal{RL})^{k-1}, \qquad \underline{\mathcal{L}}\mathcal{R}\underline{\mathcal{R}}(\mathcal{LR})^{k-1}. \tag{32}$$

Therefore, the hidden cycles appearing at the border collision bifurcations $\xi^{\mathcal{L}}_{\mathcal{LR}}$ and $\xi^{\mathcal{R}}_{\mathcal{LR}}$ are associated with the symbolic sequences

$$\varkappa^{\mathcal{L}}(\underline{\mathcal{R}}\mathcal{L}\underline{\mathcal{L}}(\mathcal{RL})^{k-1}) \equiv \mathcal{C}(\mathcal{RL})^k, \qquad \varkappa^{\mathcal{R}}(\underline{\mathcal{L}}\mathcal{R}\underline{\mathcal{R}}(\mathcal{LR})^{k-1}) \equiv \mathcal{C}(\mathcal{LR})^k \tag{33}$$

respectively. As before, the points of these cycles are given by the pre-images of zero and each of the hidden cycles exists under the conditions that all the relevant pre-images are located inside the invariant absorbing interval $[\mu_{\mathcal{R}}, \mu_{\mathcal{L}}]$. It follows from (ii), (iii) that for each $k \geqslant 1$ the hidden cycles $\mathcal{O}_{\mathcal{C}(\mathcal{RL})^k}$ $\mathcal{O}_{\mathcal{C}(\mathcal{LR})^k}$ exist in the parameter intervals

$$\left[\xi^{\mathcal{L}}_{\mathcal{L}(\mathcal{LR})^k},\, \xi^{\mathcal{R}}_{\mathcal{LR}}\right) \quad \text{and} \quad \left(\xi^{\mathcal{L}}_{\mathcal{LR}},\, \xi^{\mathcal{R}}_{(\mathcal{LR})^k\mathcal{R}}\right] \tag{34}$$

respectively (a few examples can easily be seen in Fig. 10(a)). Moreover, as the hidden fixed point $\mathcal{O}_{\mathcal{C}}$ exists at the border collision bifurcations $\xi^{\mathcal{L}}_{\mathcal{LR}}$, $\xi^{\mathcal{R}}_{\mathcal{LR}}$, it follows from (iv) and (33) that these bifurcations lead to the appearance of hidden cycles $\mathcal{O}_{\mathcal{C}^j(\mathcal{RL})^k}$, $\mathcal{O}_{\mathcal{C}^j(\mathcal{LR})^k}$, for $j, k \geqslant 1$, respectively.

6.3. The continuous and the smooth maps: Augmented period adding

In the continuous map (3) and smooth map (4) in the limiting cases $(d_{\mathcal{R}} - d_{\mathcal{L}}) \to 0$ and $\varepsilon \to 0$, respectively, the described structure persists with the obvious modification, namely that hidden cycles become simply unstable. The discussion below applies only sufficiently close to these limits, and in this manner hidden orbits provide a first step in approximating these structures in the continuous or smooth maps, but we leave deeper study of the perturbation to $(d_{\mathcal{R}} - d_{\mathcal{L}})$ and $\varepsilon \to 0$ values away from zero to future work. Under this assumption, in the continuous map (3), all the cycles which appear hidden at a border collision bifurcation of a cycle $\mathcal{O}_\sigma$ in the connected maps (2), appear at the same bifurcation as well. As an example, Fig. 11(a) shows the appearance of the fixed point $\mathcal{O}_{\mathcal{C}}$ (at the border collision bifurcations $\xi^{\mathcal{L}}_{\mathcal{L}}$ and $\xi^{\mathcal{R}}_{\mathcal{R}}$ of the fixed points), the 2-cycle $\mathcal{O}_{\mathcal{CL}}$ (at the border collision bifurcations $\xi^{\mathcal{L}}_{\mathcal{L}}$ and $\xi^{\mathcal{R}}_{\mathcal{LR}}$), and the 2-cycle $\mathcal{O}_{\mathcal{CR}}$ (at $\xi^{\mathcal{R}}_{\mathcal{R}}$ and $\xi^{\mathcal{L}}_{\mathcal{LR}}$). Similarly, in Fig. 11(b) six 3-cycles are shown, namely $\mathcal{O}_{\mathcal{CL}^2}$, $\mathcal{O}_{\mathcal{CR}^2}$, $\mathcal{O}_{\mathcal{CLR}}$, $\mathcal{O}_{\mathcal{CRL}}$, $\mathcal{O}_{\mathcal{C}^2\mathcal{L}}$, and $\mathcal{O}_{\mathcal{C}^2\mathcal{R}}$. Among these 3-cycles,

- the cycles $\mathcal{O}_{\mathcal{CL}^2}$, $\mathcal{O}_{\mathcal{CR}^2}$ are associated with the symbolic sequences $\varkappa^{\mathcal{R}}(\mathcal{RL}^2)$ and $\varkappa^{\mathcal{L}}(\mathcal{LR}^2)$ (recall that $\mathcal{RL}^2$ and $\mathcal{LR}^2$ are the only children sequences with the length 3 of $\mathcal{L}$ and $\mathcal{R}$, respectively). Therefore, the cycle $\mathcal{O}_{\mathcal{CL}^2}$ exists between the border collision bifurcations $\xi^{\mathcal{L}}_{\mathcal{L}}$ and $\xi^{\mathcal{R}}_{\mathcal{RL}^2}$ and the cycle $\mathcal{O}_{\mathcal{CL}^2}$ between $\xi^{\mathcal{R}}_{\mathcal{R}}$ while $\xi^{\mathcal{L}}_{\mathcal{LR}^2}$.
- the cycles $\mathcal{O}_{\mathcal{CLR}}$, $\mathcal{O}_{\mathcal{CRL}}$ are associated with the symbolic sequences $\varkappa^{\mathcal{L}}(\mathcal{RL}^2)$ and $\varkappa^{\mathcal{R}}(\mathcal{LR}^2)$, respectively. As $\mathcal{RL}^2$ and $\mathcal{LR}^2$ are children sequences of $\mathcal{LR}$ the existence interval of the cycle $\mathcal{O}_{\mathcal{CLR}}$ is confined by the border collision bifurcations $\xi^{\mathcal{L}}_{\mathcal{RL}^2}$, $\xi^{\mathcal{R}}_{\mathcal{RL}}$ and the existence interval of $\mathcal{O}_{\mathcal{CRL}}$ by $\xi^{\mathcal{R}}_{\mathcal{LR}^2}$ and $\xi^{\mathcal{L}}_{\mathcal{LR}}$.
- the cycles $\mathcal{O}_{\mathcal{C}^2\mathcal{L}}$, and $\mathcal{O}_{\mathcal{C}^2\mathcal{R}}$ are associated with the symbolic sequences given by concatenations of $\mathcal{C}$ with $\mathcal{CL}$ and $\mathcal{CR}$, respectively. Accordingly, the cycle $\mathcal{O}_{\mathcal{C}^2\mathcal{L}}$ exists if both the hidden fixed point $\mathcal{O}_{\mathcal{C}}$ and the hidden 2-cycle $\mathcal{O}_{\mathcal{CL}}$ exist. Since $\mathcal{O}_{\mathcal{C}}$ exists in the complete parameter interval between $\xi^{\mathcal{L}}_{\mathcal{L}}$ and $\xi^{\mathcal{R}}_{\mathcal{R}}$, while $\mathcal{O}_{\mathcal{CL}}$ does only between $\xi^{\mathcal{L}}_{\mathcal{L}}$ and $\xi^{\mathcal{R}}_{\mathcal{LR}}$, the existence region of the hidden 3-cycle $\mathcal{O}_{\mathcal{C}^2\mathcal{L}}$ coincides with the existence region of the hidden 2-cycle $\mathcal{O}_{\mathcal{CL}}$. Similarly, $\mathcal{O}_{\mathcal{C}^2\mathcal{R}}$ exists in the same parameter interval as $\mathcal{O}_{\mathcal{CR}}$.

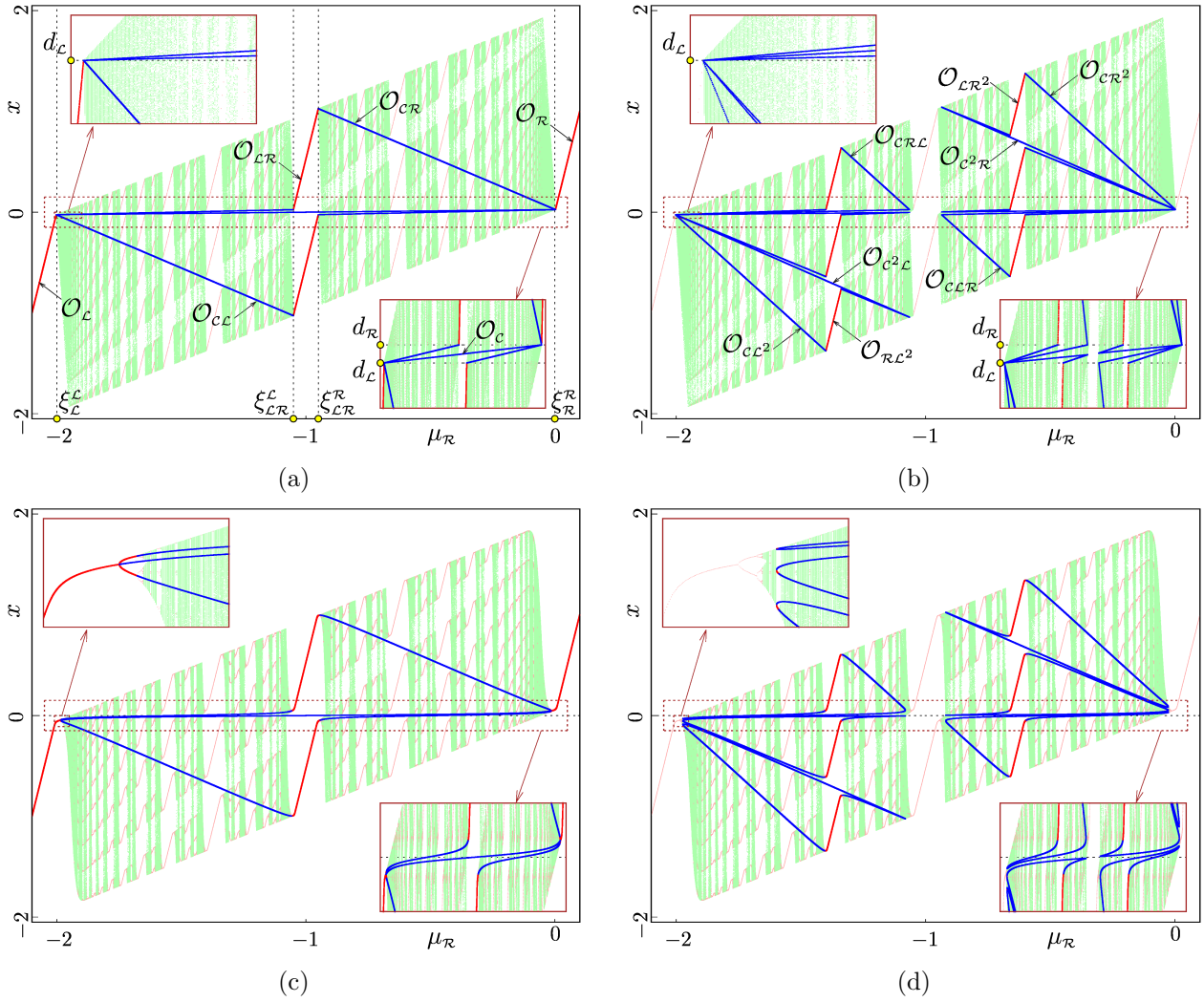

Figure 11. Bifurcations shown in (a)-(b) for the continuous map (3), and in (c)-(d) for the smooth map (4), corresponding to those of the connected map (2) from Fig. 10. Fixed points and 2-cycles are shown in (a) and (c), 3-cycles are shown in (b) and (d). Insets show magnifications of the marked rectangular regions. Shown for the parameter values from Fig. 10 with $\varepsilon = 0.1$, $d_{\mathcal{L}} = -0.025$, $d_{\mathcal{R}} = 0.025$. These diagrams more closely resemble Fig. 10 as we let $\varepsilon \to 0$ and $d_{\mathcal{L}} = -d_{\mathcal{R}} \to 0$.

In the smooth map (4), the overall bifurcation structure remains similar, although the cycles appear not in border collision but in smooth flip and fold bifurcations. It can clearly be seen in Fig. 11(c) that the 2-cycle appearing in a flip bifurcation of the fixed point $\mathcal{O}_{\mathcal{L}}$ has one point located close to zero and the other point far away from zero in the negative domain. Accordingly, this 2-cycle can be referred to as $\mathcal{O}_{\mathcal{CL}}$. For increasing $\mu_{\mathcal{R}}$ the cycle undergoes one more flip bifurcation, becomes stable with both points located far away from zero, i.e., resembling $\mathcal{O}_{\mathcal{LR}}$. Next, the cycle undergoes one more flip bifurcation, turns eventually into

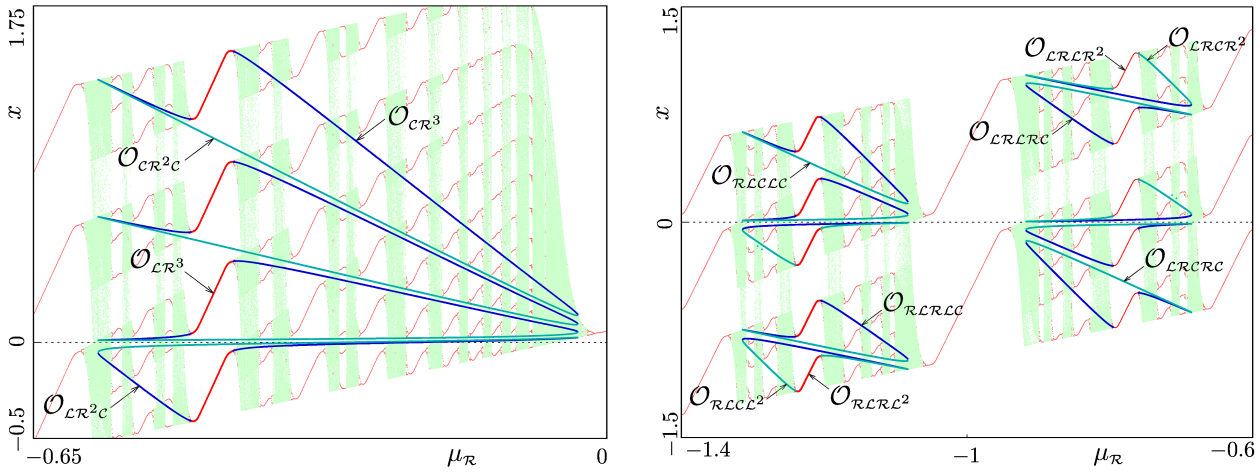

Figure 12. Generic bifurcation patterns formed by one stable and 3 unstable cycles in the smooth map (4), showing: (a) 4-cycles, and (b) 5-cycles; for parameter values $a_{\mathcal{L}} = a_{\mathcal{R}} = 0.9$, $\mu_{\mathcal{L}} = \mu_{\mathcal{R}} + 2$, $\varepsilon = 0.1$.

$\mathcal{O}_{\mathcal{C}\mathcal{R}}$, and finally disappears in a flip bifurcation of the fixed point $\mathcal{O}_{\mathcal{R}}$.

Similar transformations of 3-cycles of map (4) are illustrated in Fig. 11(d). By contrast to the 2-cycle, these appear and disappear via fold bifurcations, but the overall structure remains similar to the one in map (3), as both structures follow the same generic template defined by the corresponding (hidden and non-hidden) cycles in the connected map (2).

It is also worth noticing that each cycle $\mathcal{O}_{\varrho\sigma}$ which appear stable in the period adding structure in the discontinuous map (1) is involved, in the continuous map (3) and smooth map (4), into a generic pattern formed by four cycles of the same period. Two of these cycles (which are hidden in map (2)), namely $\mathcal{O}_{\varkappa^{\mathcal{L}}(\varrho\sigma)}$ and $\mathcal{O}_{\varkappa^{\mathcal{R}}(\varrho\sigma)}$ have already been discussed above, and it has been mentioned that these cycles appear (in map (2)) at the border collision bifurcations $\xi_\sigma^{\mathcal{R}}$ and $\xi_\varrho^{\mathcal{L}}$. Additionally, at the same bifurcations one more cycle of the same period appears. Clearly, as this cycle is complementary both to $\mathcal{O}_{\varkappa^{\mathcal{L}}(\varrho\sigma)}$ and $\mathcal{O}_{\varkappa^{\mathcal{R}}(\varrho\sigma)}$, the associated symbolic sequence is

$$\varkappa^{\mathcal{L}}(\varkappa^{\mathcal{R}}(\varrho\sigma)). \tag{35}$$

As an example, Fig. 12(a) shows this pattern for the 4-cycle $\mathcal{O}_{\mathcal{L}\mathcal{R}^3}$ in map (4). The symbolic sequences of all four involved cycles are provided by the following diagram:

$$\begin{array}{ccc} & \underline{\mathcal{L}}\mathcal{R}\mathcal{R}\underline{\mathcal{R}} & \\ \swarrow & & \searrow \\ \underline{\mathcal{L}}\mathcal{R}\mathcal{R}\underline{\mathcal{C}} & & \underline{\mathcal{C}}\mathcal{R}\mathcal{R}\underline{\mathcal{R}} \\ \searrow & & \swarrow \\ & \underline{\mathcal{C}}\mathcal{R}\mathcal{R}\underline{\mathcal{C}} & \end{array} \tag{36}$$

Similarly, for the patterns related to 5-cycles $\mathcal{O}_{\mathcal{LRLR}^2}$ and $\mathcal{O}_{\mathcal{RLRL}^2}$ of map (4) shown in Fig. 12(b), the corresponding diagrams are given by

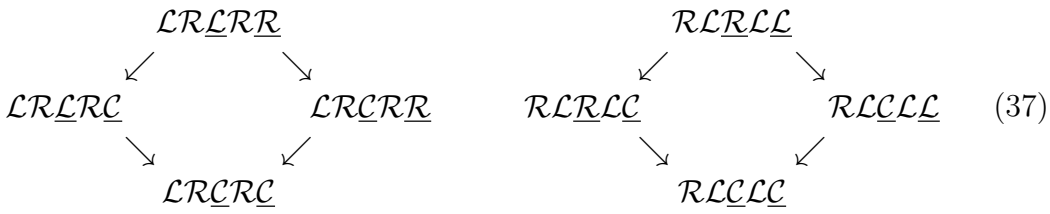

(37)

6.4. The different maps compared

As in the examples discussed earlier, the bifurcation structures in the continuous map (3) and in the smooth map (4) are more complicated than the one in the discontinuous map (1). As already mentioned, the standard period adding structure in map (1) is formed by attracting cycles and Cantor set attractors. In maps (3) and (4), no Cantor set attractor exists, and not every attracting cycle existing in map (1) is present in maps (3) and (4). Instead, these maps exhibit other invariant sets, in particular, attracting and repelling cycles, chaotic attractors and repellers.

Indeed, an attractor existing in the discontinuous map (1) is preserved in the continuous map (3) iff its points are located sufficiently far away from the border point $x = 0$. Therefore, a transition from map (1) to map (3) destroys all Cantor set attractors and also many attracting cycles (since these appear via border collision bifurcations at $x = 0$, sufficiently close to these bifurcations a point of any cycle of map (1) is close to $x = 0$). Instead, map (3) exhibits repelling cycles and moreover, robust chaotic attractors containing points located on the middle partition $(d_{\mathcal{L}}, d_{\mathcal{R}})$. As for the smooth map (4), is has non-robust chaotic attractors as well as stable cycles with some points located sufficiently close to its smooth local minimum and maximum surrounding the middle (steep) branch of the function. However, as maps (3) and (4) approach map (2), i.e., for $(d_{\mathcal{R}} - d_{\mathcal{L}}) \to 0$ and $\varepsilon \to 0$, respectively, the portion of the parameter space occupied by chaotic attractors and stable cycles (but but the parameter intervals associated with repelling cycles) tends to zero measure. Therefore, the augmented period adding bifurcation structure we reported above for map (2) is the limiting case of the bifurcation structures in maps (3) and (4). Evidently, it includes all the stable cycles existing in map (1), and all the unstable cycles existing in maps (3) and (4) in the limiting cases $(d_{\mathcal{R}} - d_{\mathcal{L}}) \to 0$ and $\varepsilon \to 0$, respectively. A great advantage of map (2) is that all its unstable cycles, being given by pre-images or zero, can be calculated much easier than the corresponding unstable orbits of the continuous and smooth maps (omitted for that very reason). Already for this reason, the connected map provides a useful approximation of the continuous and smooth maps. Moreover, the diagrams (36) and (37) above show how intuitively simple hidden orbits can be specified and tracked through border collisions, showing the organizing principles of the overall bifurcation structure.

7. Discussion: the role of hidden orbits

In section 4 to section 6, we have seen how hidden orbits provide unstable structures that help define the structure of bifurcation diagrams for maps with discontinuities. In section 4 to section 5, the results are intuitively consistent with standard bifurcations, suggesting that a topological equivalence may be possible between connected and continuous maps. The more important conclusion is that we can carry out such a bifurcation analysis entirely within the connected map, using hidden orbits and their concatenations, without reference to continuous or any such equivalence being necessary.

We have shown examples of continuous and smooth maps here merely to show qualitatively the correspondence between the bifurcations of the connected and continuous maps. Regularizations that seek a continuous map equivalent in some limit to a discontinuous map are non-unique, in terms of the gradients of the continuous maps sought and their order of differentiability, and even how the limit is defined in which the discontinuity forms. Notably, however, our results suggest that in the limit there exists a well-defined structure, and that it is uniquely defined by the connected map.

In section 6, we saw not only how hidden orbits can be used to gain more information about the structure of cascades known to occur in discontinuous maps, but also that this limit can be used to study (as an approximation) the bifurcations of steep continuous maps that have not been studied to date.

The results for the simple bifurcations in section 4 to section 5 in hindsight seem intuitive, and perhaps even obvious: given that the connected map is clearly the limit of *some* continuous map, as a segment of that map becomes increasingly steep, unstable orbits visiting that segment will bunch up until they lie on the discontinuity. What is not obvious is that this limiting behaviour should be useful, i.e. that it should provide well-defined orbits, but we have shown that hidden orbits provide precisely that, sequences of orbits that unambiguously form well-defined branches of bifurcation diagrams. Importantly, the concatenations of hidden orbits are vital to this, despite having peculiar properties such as the fact they they overlap and are infinitely unstable.

Maps with discontinuities continue to find new applications in science and engineering, from early abstract models to study chaos such as [28], to now appearing in the study of grazing in impact oscillators such as [29], or due to grazing in models of homeostasis in sleep-wake processes such as [30]. Examples like these exhibit a wide range of bifurcation sequences like those studied here, but in which the presence of hidden orbits is yet to be studied. In many cases like the impact maps in [29] and sleep-wake maps in [30], more detailed physical modeling can suggest that a discontinuous map is merely an approximation for a continuous function, and little study has so far been made of the bifurcations of those continuous and typically highly nonlinear maps, for which connected maps and their hidden orbits, rather than strictly discontinuous maps, may provide a useful first approximation.

Interestingly, in order to usefully characterize the dynamics, hidden orbits do not necessarily need to represent physically accessible states of the system being modelled. In the example of the flip bifurcation in Fig. 2, the hidden orbit defines the basin boundary of the attractors. For a given application such an orbit need not necessarily represent a physical motion, but might occupy a region of state space that is not reachable physically, or may only be a pseudo-trajectory of the system. For example, in the return maps derived from Lorenz or Cherry flows [1, 2, 3, 4], a hidden orbit corresponds to a pseudo-trajectory that passes through a saddlepoint between different branches of its stable and unstable manifolds, not a proper orbit of the flow itself, and yet significant in defining a region of orbits that are not accessible in the return map.

8. Closing remarks

We have presented the first steps towards an understanding of bifurcations in discontinuous maps where the discontinuity is treated as a connecting vertical (i.e. set-valued) branch. We have shown, as suggested in [16], that hidden orbits in such maps simplify the description of these bifurcations by bringing them closer to the familiar bifurcations of continuous maps. In particular, we have shown here how behaviours special to discontinuous maps — involving border collisions where periodic points are seemingly able to appear as if from nowhere, in finite or infinite quantities, or accumulating as infinite sub-sequences of such bifurcations — fit with the behaviour of continuous maps when hidden orbits are taken into account.

It is worth emphasizing that the connected map, and the introduction of hidden orbits, do not undo what has been done in the study of discontinuous maps to date, indeed quite the contrary. As remarked earlier (in section 2.2), adding connectedness across the discontinuity only adds to, not subtracts from or alters, the bifurcation structures known from discontinuous maps.

What this does suggest, however, is that a more rigorous correspondence could be proven to exist between the dynamics of connected discontinuous maps and continuous or differentiable maps with a steep branch. This permits more rigorous and complete use of piecewise-linear maps to approximate smooth nonlinear maps with steep changes.

The obvious advantage of piecewise-linear maps is that their orbits and bifurcations can be expressed explicitly and exactly. Were one to analyze the smooth map presented here for its own sake, it would be difficult to provide a complete description of its intricate and densely crowded bifurcation structures. The connected map, on the other hand, has a bifurcation structure that can be described explicitly and is easy to characterize. That structure is partly described by standard theory of discontinuous maps, but the connected map ensures that the full topological bifurcation structure of the smooth map (in particular highly unstable orbits created by the steep branch) is preserved.

The clearest demonstration of this is in section 4 and Fig. 2. The border collision

bifurcations seen in Fig. 2(a) are not in any way comparable to the bifurcations of continuous maps, and yet simply by including the discontinuity as a connecting vertical branch, we obtain the 'hidden orbits' of the discontinuous maps by which the bifurcations in Fig. 2(b) are recognisable simply as fold and flip bifurcations, clearly approximating the fold and flip bifurcations of the continuous and smooth maps in Fig. 2(c)-(d).

In section 4, omitting hidden orbits would miss only a small number of unstable branches that help complete the bifurcation diagrams. In section 5 and section 6, by contrast, omitting hidden orbits would miss an infinity of unstable branches, including a chaotic repeller in section 5 and section 6. Accepting the set-valuedness of the connected map would seem to be a small price to pay to restore these features in the form of hidden orbits. In the period adding structure, we have shown how to provide a complete specification of all the existing hidden orbits using the parent-child relationship in the symbolic sequence adding scheme.

A more ambitious goal in the future would be to derive estimates of how far the orbits of a smooth map with a vertical branch lie from the hidden orbits of its discontinuous approximation. At the very least, the connected map can provide initial values from which to seek numerical solutions of a smooth map. But ultimately it may be possible to derive asymptotic approximations of solutions of smooth maps, which to leading order are just the solutions of a connected but discontinuous map, as suggested in [31] for the corresponding situation in dynamical flows.

We can also turn this picture around, and ask what continuous maps can tell us about discontinuous ones. Continuity is of course a powerful property in forming theorems for dynamical systems, and much of the extensive theory that exists for continuous maps is not known to hold in the presence of discontinuity. The well-known proofs of the Sharkovsky ordering for continuous maps, for example, do not hold for the discontinuous map (1), yet in [16] the ordering is conjectured to hold for the connected map (2). Indeed we expect, based on the results we have presented here, that many important theorems of dynamical systems can be extended to require only connectedness rather than continuity, something which would substantially increase their applicability to nonlinear dynamical systems. This approach follows the philosophy that A.F. Filippov applied so successfully to flows with discontinuities (as remarked in [16]), but which has taken longer to be turned systematically to maps with discontinuities. The promise that such extensions are possible is lent weight by the results here, which show how closely the connected map reproduces all of the periodic structures of continuous or smooth maps, through the most intricate of bifurcations.

Acknowledgments

The work of V. Avrutin was supported by the German Research Foundation within the scope of the project "Generic bifurcation structures in piecewise-smooth maps with extremely high number of borders in theory and applications for power converter systems".

References

[1] J. Guckenheimer and R.F. Williams. Structural stability of Lorenz attractors. *Publ. Math. IHES*, 50:59–72, 1979.

[2] R.F. Williams. The structure of Lorenz attractors. *Publ. Math. IHES*, 50:73–99, 1979.

[3] M. Martens, S. Van Strien, W. De Melo, and P. Mendes. On Cherry flows. *Ergod. Th. & Dynam. Sys.*, 10(3):531–554, 1990.

[4] J. Yang. Cherry flow: physical measures and perturbation theory. *Ergod. Th. & Dynam. Sys.*, 37(8):2671–88, 2017.

[5] J-J. E. Slotine and W. Li. *Appl. Nonlin. Control*. Prentice Hall, 1991.

[6] C. Edwards and S. K. Spurgeon. *Sliding Mode Control*. Taylor & Francis, 1998.

[7] J. Shi, J. Guldner, and V. I. Utkin. *Sliding mode control in electro-mechanical systems*. CRC Press, 1999.

[8] M. P. Bailey, G. Derks, and A. C. Skeldon. Circle maps with gaps: Understanding the dynamics of the two-process model for sleep–wake regulation. *Europ. J. Appl. Math.*, 29(5):845–68, 2018.

[9] M. R. Jeffrey and H. Dankowicz. Discontinuity-induced bifurcation cascades in flows and maps with application to models of the yeast cell cycle. *Physica D*, 271:32–47, 2014.

[10] M. di Bernardo, C. J. Budd, A. R. Champneys, and P. Kowalczyk. *Piecewise-smooth Dynamical Systems: Theory and Applications*, volume 163 of *Applied Mathematical Sciences*. Springer, 2008.

[11] V. Avrutin, L. Gardini, I. Sushko, and F. Tramontana. *Continuous and Discontinuous Piecewise-Smooth One-dimensional Maps: Invariant Sets and Bifurcation Structures*. Nonlinear Science, Series A. World Scientific, 2019.

[12] S. J. Hogan, L. Higham, and T. C. L. Griffin. Dynamics of a piecewise linear map with a gap. *Proc. R. Soc. A*, 463:49–65, 2007.

[13] J. Andres. Period two implies chaos for a class of multivalued maps: a naive approach. *Computers & Math. Appl.*, 64(7):2160–5, 2012.

[14] L. Alvin, and J. Kelly. Topological entropy of Markov set-valued functions. *Ergod. Th. & Dynam. Sys.*, 41(2):321-337, 2021.

[15] V. Avrutin and M. Schanz. On the fully developed bandcount adding scenario. *Nonlinearity*, 21:1077–1103, 2008.

[16] M. Jeffrey and S. Webber. The hidden unstable orbits of maps with gaps. *Proc. R. Soc. A*, 476(2234):20190473, 2020.

[17] V. Avrutin and M. Schanz. Period-doubling scenario without flip bifurcations in a one-dimensional map. *Int. J. Bifurcation Chaos*, 15(4):1267–84, 2005.

[18] R. I. Leine, D. H. van Campen, and C. Glocker. Nonlinear dynamics and modeling of various wooden toys with impact and friction. *J. Vibr. Contr.*, 9:25–78, 2003.

[19] A. Panchuk, I. Sushko, B. Schenke, and V. Avrutin. Bifurcation structures in a bimodal piecewise linear map: regular dynamics. *Int. J. Bifurcation Chaos*, 23(12):1330040, 2013.

[20] A. Panchuk, I. Sushko, and V. Avrutin. Bifurcation structures in a bimodal piecewise linear map: chaotic dynamics. *Int. J. Bifurcation Chaos*, 25(3), 2015.

[21] M. Jeffrey. *Hidden Dynamics: The Mathematics of Switches, Decisions and Other Discontinuous Behaviour*. Springer, 2018.

[22] N. N. Leonov. On a pointwise mapping of a line into itself. *Radiofisika*, 2(6):942–956, 1959. (in Russian).

[23] O. Feely and L. O. Chua. Nonlinear dynamics of a class of analog-to-digital converters. *Int. J. Bifurcation Chaos*, 22(2):325–340, 1992.

[24] N. N. Leonov. On a discontinuous piecewise-linear pointwise mapping of a line into itself. *Radiofisika*, 3(3):496–510, 1960. (in Russian).

[25] N. N. Leonov. On the theory of a discontinuous mapping of a line into itself. *Radiofisika*, 3(5):872–886, 1960. (in Russian).

[26] C. Haros. Tables pour évaluer une fraction ordinaire avec autant de decimales qu'on voudra; et pour trouver la fraction ordinaire la plus simple, et qui approche sensiblement d'une fraction décimal. *J. de L'Ecole Royale Polytechnique*, IV(11):364–368, 1802.

[27] A.-L. Cauchy. Démonstration d'un théorème curieux sur les nombres. In *Oeuvres complètes*, volume 2 of *Cambridge Library Collection - Mathematics*, pages 207–209. Cambridge University Press, 2009.

[28] E. N. Lorenz. Deterministic nonperiodic flow. *Journal of the Atmospheric Sciences*, 20(2):130–41, 1963.

[29] H. Jiang, A. S. E. Chong, Y. Ueda, and M. Wiercigroch. Grazing-induced bifurcations in impact oscillators with elastic and rigid constraints. *Int. J. Mech. Sci.*, 127:204–14, 2017.

[30] M. P. Bailey, G. Derks, and A. C. Skeldon. Circle maps with gaps: Understanding the dynamics of the two-process model for sleep-wake regulation. *Europ. J. Appl. Math.*, 29(5):845–68, 2018.

[31] M. R. Jeffrey. *Modeling with nonsmooth dynamics*. Frontiers in Applied Dynamical Systems. Springer Nature Switzerland, 2020.

Appendix A. Classification of the maps

If ones seeks a complete classification of the bifurcations of the map (2) (or equivalently of (1) or (3) or (4)), there are 32 distinct generic classes to consider, associated with different stabilities of the three branches of the map (i.e. left, right, and vertical). These come from having four cases for each slope $a_{\mathcal{R}}$ and $a_{\mathcal{L}}$, namely whether they are positive or negative and have modulus greater or less than unity, while the two possible signs of $\mu_{\mathcal{L}} - \mu_{\mathcal{R}}$ determine whether the map has a 'negative jump' or 'positive jump' (i.e. a slope of $+\infty$ or $-\infty$) at $x = 0$.

These generic classes can be represented as follows in Figures A1 and A2. Within these we can identify monotonic shapes (classes 1,2,5,6,27,28,31,32), unimodal shapes (classes 3,4,7–10,13,14,19,20,23–26,29,30), and bimodal shapes (classes 11,12,15–18,21,22). Each is shown at the bifurcation value $\mu_{\mathcal{R}} = 0$. Sections 4, 5, and 6, show examples taken from the cases 27, 8, and 22, respectively.

Unfortunately, while we include these as a useful starting point for more general bifurcation analyses, there is no simple connection between the slopes defining these classes and the bifurcations they exhibit. It is not even simple to derive whether the bifurcations in each class are local or global without some analysis. In a continuous map a border collision bifurcation is always local, since all the orbits involved in the bifurcation are located in a set of small intervals around the border point and its pre-images, and these all shrink to zero size as the bifurcation value is approached. In discontinuous maps, regardless of the slopes outside of the discontinuity, this localization no longer holds, because the jump at the discontinuity prevents these intervals shrinking to zero. As a result, border collisions in discontinuous maps may be global as well as local, and this remains so in the connected form (2).

A more useful classification would therefore consider the number of rank-one pre-images of $x = 0$ before and after a bifurcation. In the connected map (2) this number may be zero,

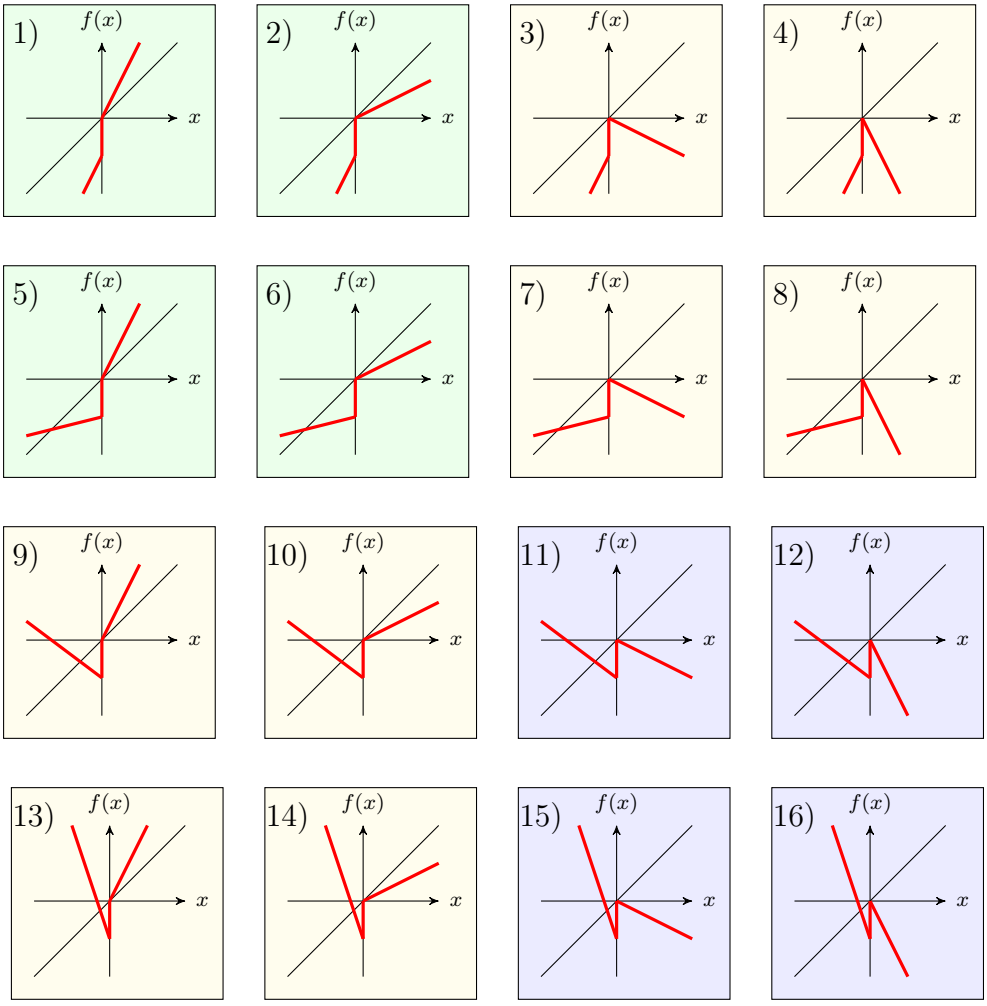

Figure A1. Generic shapes of map (2) in the "positive jump" configuration.

one, two, or three (including that $x = 0$ can map to itself). Note that only those pre-images that are reachable from the interval J are involved in the creation of hidden orbits. Hence a classification may be based on the number of pre-images of zero (of any rank) appearing at a bifurcation inside J. If, for example, this number increases from zero to one, the bifurcation leads to the appearance of a single hidden orbit. But if at least two pre-images appear inside J at the bifurcation, this leads immediately to the appearance of an infinite number of periodic and aperiodic hidden orbits (see section 3.3).

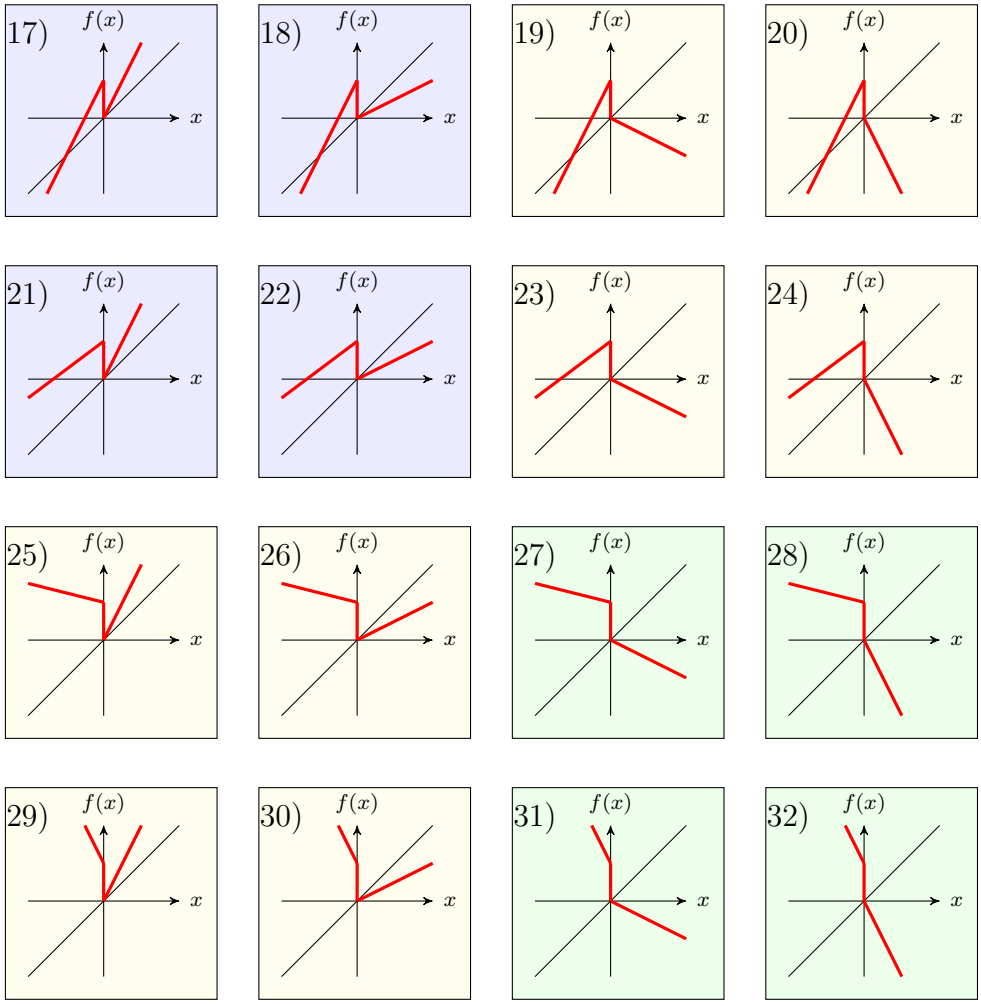

Figure A2. Generic shapes of map (2) in the "negative jump" configuration.